Pure appl. geophys. 163 (2006) 567–600
0033–4553/06/030567–33
DOI 10.1007/s00024-005-0034-6

Pure and Applied Geophysics

Temporal Changes of Shallow Seismic Velocity Around the Karadere-Düzce Branch of the North Anatolian Fault and Strong Ground Motion

ZHIGANG PENG,[1,2] and YEHUDA BEN-ZION[1]

Abstract—We analyze temporal variations of seismic velocity along the Karadere-Düzce branch of the north Anatolian fault using seismograms generated by repeating earthquake clusters in the aftershock zones of the 1999 M_w7.4 İzmit and M_w7.1 Düzce earthquakes. The analysis employs 36 sets of highly repeating earthquakes, each containing 4–18 events. The events in each cluster are relocated by detailed multi-step analysis and are likely to rupture approximately the same fault patch at different times. The decay rates of the repeating events in individual clusters are compatible with the Omori's law for the decay rate of regional aftershocks. A sliding window waveform cross-correlation technique is used to measure travel time differences and evolving decorrelation in waveforms generated by each set of the repeating events. We find clear step-like delays in the direct *S* and early *S*-coda waves (sharp seismic velocity reduction) immediately after the Düzce main shock, followed by gradual logarithmic-type recoveries. A gradual increase of seismic velocities is also observed before the Düzce main shock, probably reflecting post-seismic recovery from the earlier İzmit main shock. The temporal behavior is similar at each station for clusters at various source locations, indicating that the temporal changes of material properties occur in the top most portion of the crust. The effects are most prominent at stations situated in the immediate vicinity of the recently ruptured fault zones, and generally decrease with normal distance from the fault. A strong correlation between the co-seismic delays and intensities of the strong ground motion generated by the Düzce main shock implies that the radiated seismic waves produced the velocity reductions in the shallow material.

Key words: Seismic velocity changes, crustal structure, scattering, coda waves, repeating earthquakes, strong ground motion.

1. Introduction

Laboratory experiments and theory indicate that the elastic properties of crustal rocks evolve when the stress-strain conditions are beyond those associated with the linear elastic regime (e.g., MOGI, 1962; SCHOLZ, 1968; JAEGER and COOK, 1976;

[1]Department of Earth Sciences, University of Southern California, Los Angeles, CA, 90089-0740, USA
[2]Department of Earth and Space Sciences, University of California, Los Angeles, CA, 90095-1567, USA E-mail: zpeng@ess.ucla.edu

LOCKNER *et al.*, 1992; LYAKHOVSKY *et al.*, 1997; TEN CATE *et al.*, 2000; HAMIEL *et al.*, 2004; JOHNSON and SUTIN, 2005). Since the stress-strain fields exceed the linear elastic regime at some regions during the occurrence of earthquakes, such changes should be, in principle, measurable through seismological observations. Observing temporal variations of material properties in the seismogenic zone has been a long-sought goal of the geophysics community. In the past, three seismological approaches have been applied to measure temporal changes of crustal properties: travel time of P and S arrivals or Vp/Vs ratio (e.g., WHITCOMB *et al.*, 1973), seismic anisotropy (e.g., GUPTA, 1973; CRAMPIN *et al.*, 1990, 1991; CRAMPIN and GAO, 2005), and analysis of coda wave (e.g., AKI and CHOUET, 1975; AKI, 1985; JIN and AKI, 1986). Some studies claimed to observe fairly large temporal changes (e.g., more than 10%) using natural earthquake sources (e.g., GUPTA, 1973; Jin and AKI, 1986; CRAMPIN *et al.*, 1990). However, these claims were not convincing, mainly due to uncertainties associated with earthquake locations and origin times (e.g., MCEVILLY and JOHNSON, 1974; RYALL and SAVAGE, 1974; KANAMORI and FUIS, 1976; ASTER *et al.*, 1990, 1991; BEROZA *et al.*, 1995; HELLWEG *et al.*, 1995; ANTOLIK *et al.*, 1996; LIU *et al.*, 2004, 2005; PENG and BEN-ZION, 2005).

Recent results from controlled source studies have shown considerably smaller but detectable temporal changes (on the order of a few percent) associated with the occurrence of major earthquakes (e.g., MATSUMOTO *et al.*, 2001; VIDALE and LI, 2003; IKUTA and YAMAOKA, 2004). One advantage of controlled source studies is that the space-time coordinates of the sources are known more accurately than those associated with natural earthquakes. However, studies based on controlled sources have several disadvantages including expensive cost, inadequate temporal sampling and poor depth penetration. The latter point is especially important for studies concerned with the physics of earthquakes and faults.

An effective way of using natural earthquake sources for monitoring changes of material properties is to employ sets of events that have very similar locations and focal mechanisms. These events, referred to as repeating earthquakes, generate highly similar waveforms at recording stations and are associated with nearly identical propagation paths to the stations (e.g., POUPINET *et al.*, 1984; NADEAU *et al.*, 1994; SCHAFF *et al.*, 1998). Recent relocation techniques based on waveform cross correlation (e.g., SCHAFF *et al.*, 2004) and the double-difference algorithm (e.g., WALDHAUSER and ELLSWORTH, 2000) improved significantly the determination of relative earthquake locations. This has allowed the identification of many sets of repeating earthquake clusters, mainly along the central and northern sections of the San Andreas fault system (e.g., SCHAFF *et al.*, 1998, 2002; RUBIN, 2002; WALDHAUSER *et al.*, 2004; PENG *et al.*, 2005), and along portions of subduction zones in Japan (e.g., IGARASHI *et al.*, 2003).

Using repeating earthquakes, BOKELMANN and HARJES (2000) found $\sim$2% decrease in shear-wave anisotropy associated with a fluid injection experiment at the 9 km deep KTB borehole in Germany. NIU *et al.* (2003) detected systematic

temporal variations in early *S*-coda waves from repeating earthquakes along the Parkfield segment of the San Andreas fault. They interpreted the observation as resulting from migration of seismic scatterers due to a transient aseismic event. SCHAFF and BEROZA (2004) and RUBINSTEIN and BEROZA (2004a,b) reported clear co-seismic reduction of seismic velocity followed by logarithmic post-seismic recovery in the aftershock zones of the 1984 M6.2 Morgan Hill earthquake, the 1989 M6.9 Loma Prieta earthquake, and its largest aftershock, the 1990 M5.4 Chittenden earthquake. They suggested that the changes reflect evolution in the microcrack density in the top-most portion of the crust, initiated by the strong ground motions of the main shocks. Using repeatable seismic sources around volcanic regions, such as repeating earthquakes (YAMAWAKI *et al.*, 2004) and gas bubbles (GRET *et al.*, 2005), clear reductions of waveform cross-correlation coefficients have been found in *P*, *S* and coda waves, indicating rapid changes in the scattering properties associated with volcanic activity. Recently, repeating ultrasonic coda waves have been used to determine the nonlinear dependence of the seismic velocity in granite (SNIEDER *et al.*, 2002). Correlation analysis of the coda waves can also be used to infer relative source separation between repeating earthquakes (SNIEDER and VRIJLANDT, 2005).

PENG and BEN-ZION (2004) performed a systematic analysis of crustal anisotropy along the Karadere-Düzce branch of the North Anatolian fault (NAF), which ruptured during the 1999 M_w7.4 İzmit and M_w7.1 Düzce earthquakes. They found $\sim$1 km broad zones around the surface traces of the İzmit and Düzce main shocks with enhanced anisotropy associated with fault-parallel cracks and/or structural fabric. The belt of anisotropic rock is confined primarily to the top $\sim$3 km of the crust and surrounds $\sim$100 m wide zone of highly damaged rock acting as trapping structure for seismic fault zone waves (BEN-ZION *et al.*, 2003). Using repeating earthquake clusters, PENG and BEN-ZION (2005) investigated the fine-scale spatial and temporal variations of crustal anisotropy in the same area. Large apparent co-seismic changes (up to 30%) of shear-wave splitting delay times are observed across the time of the Düzce main shock at stations near the epicentral region. However, the changes can be mostly explained by spatial variations of the ray paths due to the changing seismicity, rather than changes in the properties of the anisotropic medium. Splitting parameters measured using repeating earthquake clusters in the area indicate at most 2% changes in delay times associated with the occurrence of the Düzce main shock.

In this study, we use the early *S*-coda waves generated by 36 repeating earthquake sequences identified by PENG and BEN-ZION (2005) to document seismic velocity changes around the time of the Düzce earthquake. The occurrence of the İzmit earthquake three months before the Düzce main shock activated many repeating earthquake sequences in the area. This provides an important data set that can be used to constrain possible temporal changes during the pre-, co-, and post-seismic periods of the Düzce main shock. As mentioned above, our related high-resolution

study of seismic anisotropy with the same data showed only small co-seismic changes, and demonstrated the lack of robust changes of anisotropy properties either before or after the Düzce main shock. In contrast, the high resolution analysis of the present work, based on travel-time changes of the *S* and early *S*-coda waves, reveals clear co- and post-seismic changes of seismic velocities manifested, respectively, as sharp velocity reductions followed by gradual (logarithmic-type) recoveries. The results also show small gradual increases of seismic velocities before the Düzce main shock, which are likely the post-seismic recoveries from the earlier İzmit main shock. The effects are observed generally at all stations, with larger amplitudes at stations in the immediate vicinity of the damaged fault zone layer of the İzmit and Düzce rupture zones.

In the following sections 2 and 3, we describe the overall data set and properties of the repeating earthquake clusters. In section 4 we use a sliding window waveform cross-correlation technique (e.g., POUPINET *et al.*, 1984; NIU *et al.*, 2003) to measure travel-time differences and evolving decorrelation in waveforms generated by the different sets of repeating earthquakes. In section 5 we analyze the evolution of the observed temporal changes, constrain the possible regions where the temporal changes occur, and investigate possible relations between the temporal changes and the strong ground motions produced by the Düzce main shock. The implications of the results to seismic properties of the crust are discussed in section 6.

2. Data

2.1. The Seismic Experiment

The analysis employs seismic waveform data sets recorded by a temporary 10-station PASSCAL seismic network (Fig. 1a) along and around the Karadere-Düzce branch of the NAF (SEEBER *et al.*, 2000; BEN-ZION *et al.*, 2003). The seismometers were deployed a week after the August 17, 1999, M_w7.4 İzmit earthquake. All 10 stations had REFTEK recorders and three-component L22 short-period sensors with a sampling frequency of 100 Hz. In addition, 8 stations (not including MO and GE) had three-component force-balance accelerometers (FBA). The deployment location was fortunate in that three month later, the November 12, 1999, M_w7.1 Düzce earthquake occurred in the same area. Our temporary seismic network straddled the rupture zones of both main shocks and recorded about 26,000 earthquakes during its six-month operational period.

The "standard" locations for the 26,000 earthquakes, used in our previous studies, were obtained with the code HYPOINVERSE (KLEIN, 1978) and station corrections. The horizontal errors of those locations are less than 1 km around the center of the network and 1–2 km near the margins. The vertical errors are somewhat

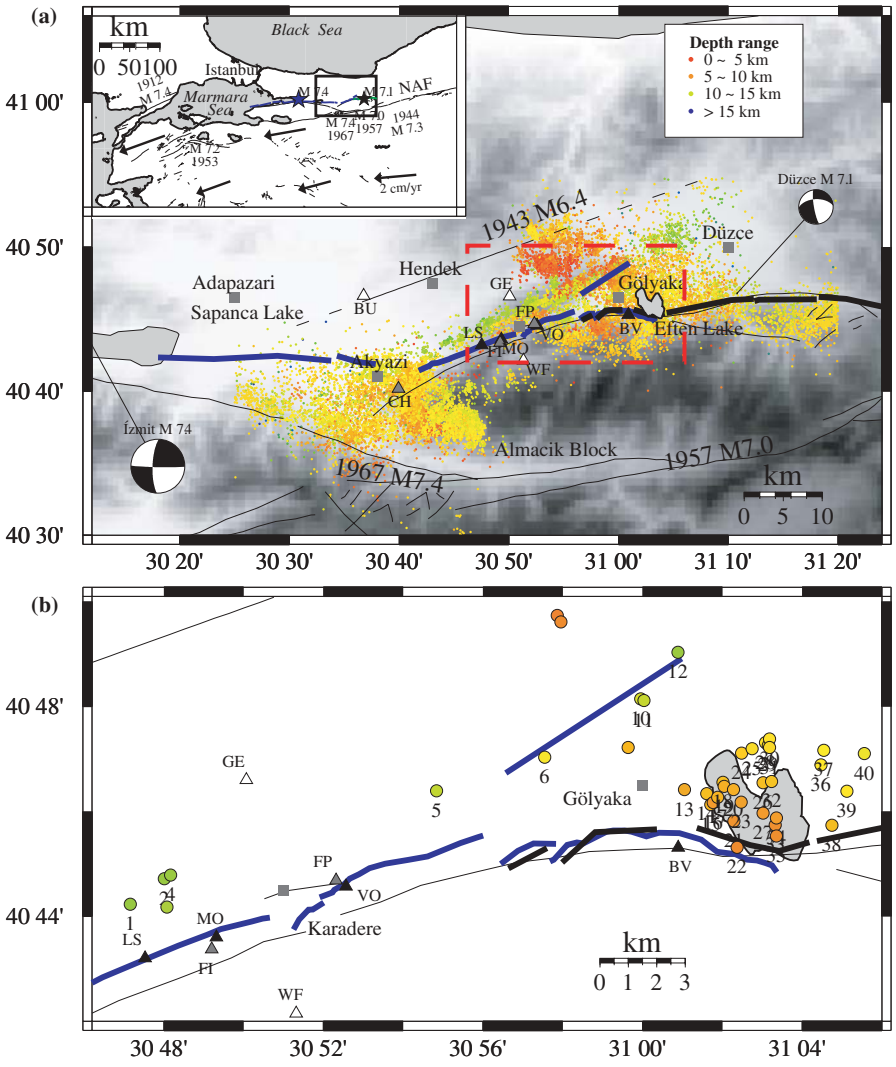

Figure 1

(a) Hypocentral distribution of ~18000 earthquakes recorded by the PASSCAL seismic experiment along the Karadere-Düzce branch of the NAF. Aftershock locations are marked by small dots with colors denoting different depth ranges. Shaded background indicates topography with white being low and dark being high. The surface ruptures of the İzmit and Düzce earthquakes are indicated with thick blue and black lines, respectively. Dark thin lines associated with earthquake information denote faults that were active during recent ruptures. Other dark thin lines are geologically inferred fault traces. Stations within, near and outside the fault zone are shaded with dark, gray and white triangles, respectively. Gray squares denote locations of nearby cities. The area bounded by the red dashed lines is shown in (b). The inset illustrates the tectonic environment in northwestern Turkey with the box corresponding to our study area. Arrow vectors represent plate deformation rate (Reilinger *et al.*, 1997) from GPS data. Modified from Peng and Ben-Zion (2005). (b) Hypocentral locations of 40 repeating event clusters in the study area. The ID is assigned to each cluster sequentially according to the centroid longitude of that cluster. The 36 clusters that are used in this study are marked by the cluster ID. Other symbols and notations are the same as in (a).

greater. Additional details regarding the seismic experiment and data set are given by SEEBER *et al.* (2000) and BEN-ZION *et al.* (2003).

PENG and BEN-ZION (2005) performed cross correlations on waveforms generated by ~18,000 earthquakes that are located within ~20 km of the temporary network and are recorded by at least 3 of the 10 stations. They identified 40 repeating earthquake clusters with a median correlation coefficient ≥ 0.95 and at least 5 events in each cluster (Fig. 1b). Among those, 28 clusters occurred around the Eften Lake, where the surface trace of the İzmit main shock terminated. Three months later, this segment reruptured during the Düzce main shock (e.g., HARTLEB *et al.*, 2002). The 28 clusters in the Eften Lake area are in the depth range of 5–10 km, and appear to be on a fault plane dipping ~65° north (UTKUCU *et al.*, 2003). The other 12 clusters are located along the Karadere segment that ruptured during the İzmit main shock. Most of these clusters are in the depth range of 10–15 km.

2.2. Hypocentral Relocation

We relocate earthquakes in each cluster using the double-difference technique (WALDHAUSER and ELLSWORTH, 2000). The technique incorporates both the catalog travel-time data and relative *P* and *S* arrival times from waveform cross correlation. The correlation measurement is obtained by a two-step procedure. We first use a 1-s time window to align *P* and *S* arrivals to a reference trace. To minimize the effect of temporal changes in the *P*- and *S*- coda waves on earthquake relocation, we then use a 0.32-s time window starting 0.12 s before the *P* arrival, and a 0.64-s time window starting 0.2 s before the *S* arrival, to compute relative travel times with subsample precision. These choices produce narrow time windows centered on the direct *P* and *S* arrivals. After relocation, the source dimensions for most earthquakes in each cluster almost overlap each other, indicating that they rupture approximately the same fault patch repeatedly (Fig. 2). However, we find a small percentage of events that are relatively far from other members of a cluster.

The events used in the analysis have magnitudes smaller than $M = 3$ (ZHU, 2003). To improve further the similarity of the employed event locations, we estimate the earthquake source dimensions using the analytical scaling relation for a circular crack in an infinite Poisson solid (e.g., KANAMORI and ANDERSON, 1975; BEN-ZION, 2003)

$$r^3 = (7/16)(P_0/\Delta\varepsilon), \tag{1}$$

where r is the crack radius, P_0 is the scalar potency of the event (given by the integral of the final slip distribution over the failure area), and $\Delta\varepsilon$ is the static strain drop of the event (equal to the ratio of a nominal stress drop divided by a nominal rigidity). To implement (1), we assume that each event sustains a strain drop of 10^{-4}

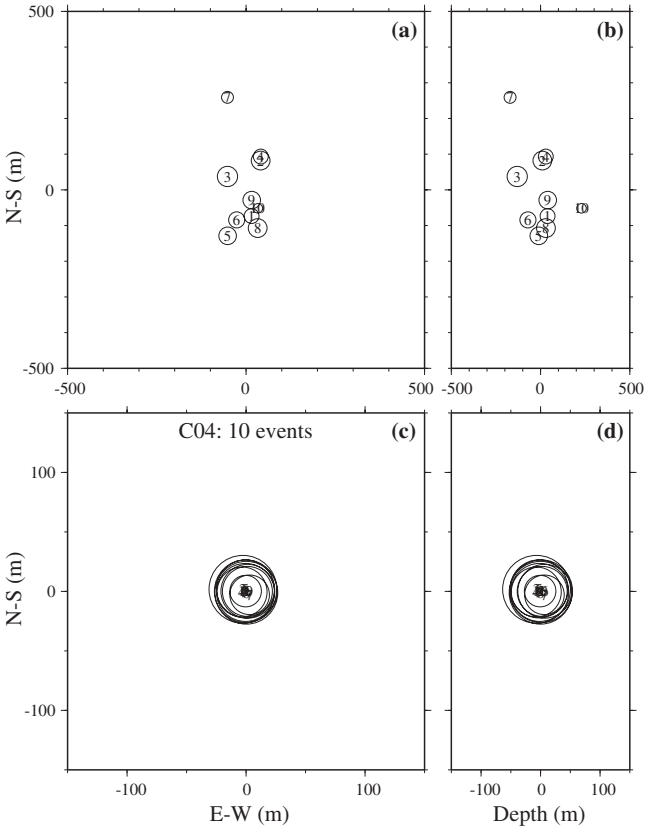

Figure 2
Map view (a) and cross section (b) of the relative locations of the 10 events in cluster C04 before relocation. Map view (c) and cross section (d) of the same 10 events after relocation. The zero coordinates correspond to the centroid location of the cluster. The circle size scales with the source radius, which is estimated based on the event magnitude (ZHU, 2003) and the potency-magnitude relation of BEN-ZION and ZHU (2002).

(KASAHARA, 1981) and employ the empirical potency-magnitude relation of BEN-ZION and ZHU (2002) for earthquakes with magnitudes $M < 3$,

$$\log P_0 = 1.00\, M - 4.72. \tag{2}$$

To ensure that only clusters of repeating events that are very close in space are used in the study of temporal changes (GOT and COUTANT, 1997), we discard an individual event if its source area does not overlap 50% with any other member in that cluster (WALDHAUSER and ELLSWORTH, 2002). This removes 25 events out of 326 events in the 40 clusters. Most of the removed events occurred during the first two weeks of the deployment when only a few of the 10 stations were installed. Consequently, their hypocenter locations are generally less well constrained. In addition, we require that

the duration of the repeating clusters is more than 10 days and that each cluster has at least four events. Clusters C03, C07, C08, and C09 do not satisfy these criteria. Ultimately, we are left with 36 clusters having 292 highly repeating events that are used for further detailed analysis.

3. Occurrence Pattern of Repeating Clusters

The remaining 36 repeating clusters in the aftershock zones of the İzmit and Düzce earthquakes are associated with sequences of failures on the same (or nearly the same) small fault patches. As shown in Fig. 3a, the recurrence intervals *Tr* of most repeating event clusters exhibit clear changes at the time of the Düzce main shock. In general, the recurrence intervals become gradually longer as the time of the Düzce main shock is approached (and the elapsed time from the earlier İzmit main shock increases), decrease sharply at the time of the Düzce main shock, and then gradually increase again after the Düzce main shock. The occurrence of the Düzce main shock affected most strongly the nearby 28 clusters in the Eften Lake area, and less so the 8 clusters that are further away along the Karadere segment.

As shown in Figure 3b, the inverse of the recurrence intervals *Tr* is approximately proportional to the elapsed times *t* since the Düzce main shock for clusters around the Eften Lake area on a log-log scale. To ensure the data quality, we select 16 out of the 28 clusters that have at least five events after the Düzce main shock, and at least a 0.8 range in the logarithm of the recurrence interval range. Since the number of repeating events in a given time interval is inversely proportional to *Tr*, each cluster of events plotted in Figure 3b is compatible individually with the empirical $1/t$ Omori law for aftershock decay rate (OMORI, 1895). However, it is important to note that the data shown in Figure 3b, covering a narrow range of time intervals, can be fitted equally well by exponential and other functions (e.g., KISSLINGER, 1996; BEN-ZION and LYAKHOVSKY, 2006). Similar patterns have been observed in the aftershock zones of the 1989 Loma Prieta earthquake (SCHAFF *et al.*, 1998) and the 1984 Morgan Hill earthquake (PENG *et al.*, 2005). The decay rates of repeating events following the Düzce main shock (and the previous İzmit event) can be explained by a variety of relaxation processes, including stress corrosion (DAS and SCHOLZ, 1981), rate- and state-dependent friction (DIETERICH, 1994), dislocation creep (ZÖLLER *et al.*, 2005) and damage rheology (BEN-ZION and LYAKHOVSKY, 2006).

The increasing rates of many repeating events at the time of the Düzce main shock provide a dense temporal sampling immediately after the Düzce event, which is very useful for a detailed study of post-seismic effects. The repeating events that were activated by the earlier İzmit main shock provide important data that can be used to study possible pre- and co-seismic changes associated with the Düzce main shock. These effects are examined in the following sections.

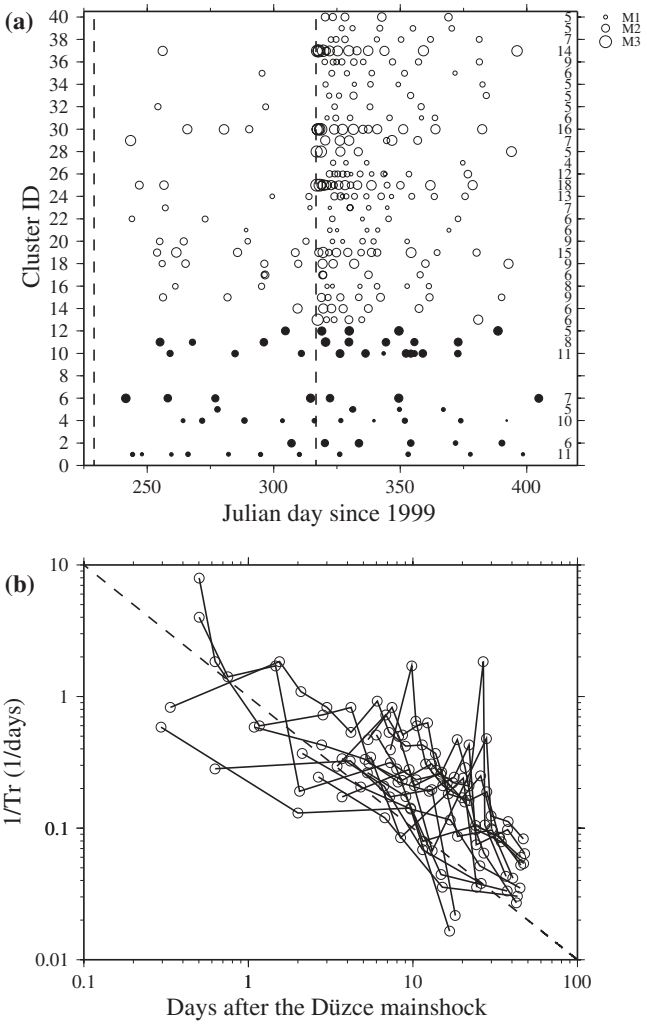

Figure 3
(a) Occurrence times (Julian day since 1999) of the 36 repeating earthquake clusters. The vertical dash lines mark the origin time of the İzmit and Düzce earthquakes. Open and filled circles mark the clusters around the Eften Lake and Karadere segment, respectively. The number of events in each cluster is marked on the right side of the figure. (b) The inverse of recurrence intervals $1/Tr$ as a function of their elapsed times t for 16 clusters near the Eften Lake that have at least 5 events after the Düzce main shock, and a range of logarithmic recurrence interval of at least 0.8. The dash line denotes the $1/t$ Omori law for aftershock decay rates.

4. Analysis Procedure

Before performing detailed analysis, we conduct the following preprocessing steps. We examine three-component data that are generated by 292 microearthquakes in 36 repeating clusters and recorded by the L22 short-period sensors. Strongly clipped seismograms are removed. The remaining seismograms are detrended, shifted to have zero mean, and bandpass filtered at 1–20 Hz using a two-pass 4-pole Butterworth filter from subroutines in the Seismic Analysis Code (GOLDSTEIN *et al.*, 2003). The bandpass filter is applied to enhance signals and remove possible incoherent noise at higher frequencies.

Next, we select for each cluster a reference seismogram that all other seismograms are compared with. We are mostly interested in temporal changes induced by the Düzce main shock, so we choose reference seismograms that are generated distant in time from the main shock, so that the influence of the Düzce main shock is small. Since our 10-station seismic network was not complete in the first several weeks of the deployment, the reference seismogram for each station is chosen to be either the last trace within each sequence, or the second-to-last if the signal-to-noise ratio for the last trace is less than 3.

The *P*- and *S*-wave arrival times are manually picked on each reference trace. The other seismograms of the repeating events in that cluster are aligned at 1 s with the manually picked *P* arrival on the reference trace. This is done by cross-correlating a 1-s-long window starting 0.2 s before the automatically picked *P* arrival on these traces (Fig. 4a). Because of this alignment, the delay times obtained from the analysis are relative to the *P* arrival of the reference trace and reflect changes in the later *S* (and *S*-coda) minus *P* time. Thus, we are unable to measure temporal changes in the *P* and early *P*-coda waves, and the obtained temporal changes from the *S* and *S*-coda waves are probably lower bounds. However, this procedure removes possible errors in the absolute timing of a seismogram (e.g., RUBINSTEIN and BEROZA, 2004a).

A sliding window waveform cross-correlation technique (NIU *et al.*, 2003) is used to measure the travel-time differences and evolving decorrelation in waveforms of the repeating earthquakes in each cluster. The delay time $\tau(t)$ and decorrelation index $D(t)$ (defined as 1 minus the maximum cross-correlation value) between the reference and subsequent seismograms are computed using a 0.5-s time window, sliding forward at 0.01 s interval through 9 s after the *P* arrival (Fig. 4). To obtain a subsample accuracy, we interpolate the waveforms from 100 samples to 10,000 samples per second. A cosine taper is applied to each window with 10% of the entire width to reduce the Gibbs' phenomenon.

Figure 4 shows clear changes of both delay time $\tau(t)$ and decorrelation index $D(t)$ for the vertical-component seismograms generated by cluster C04 and recorded at station VO. The $\tau(t)$ values at 3–4 s in the early *S*-coda waves for the earthquakes that occur before and after the Düzce main shock differ by up to 10 ms. Since the temporal evolution is most prominent in the early *S*-coda waves, we compute the

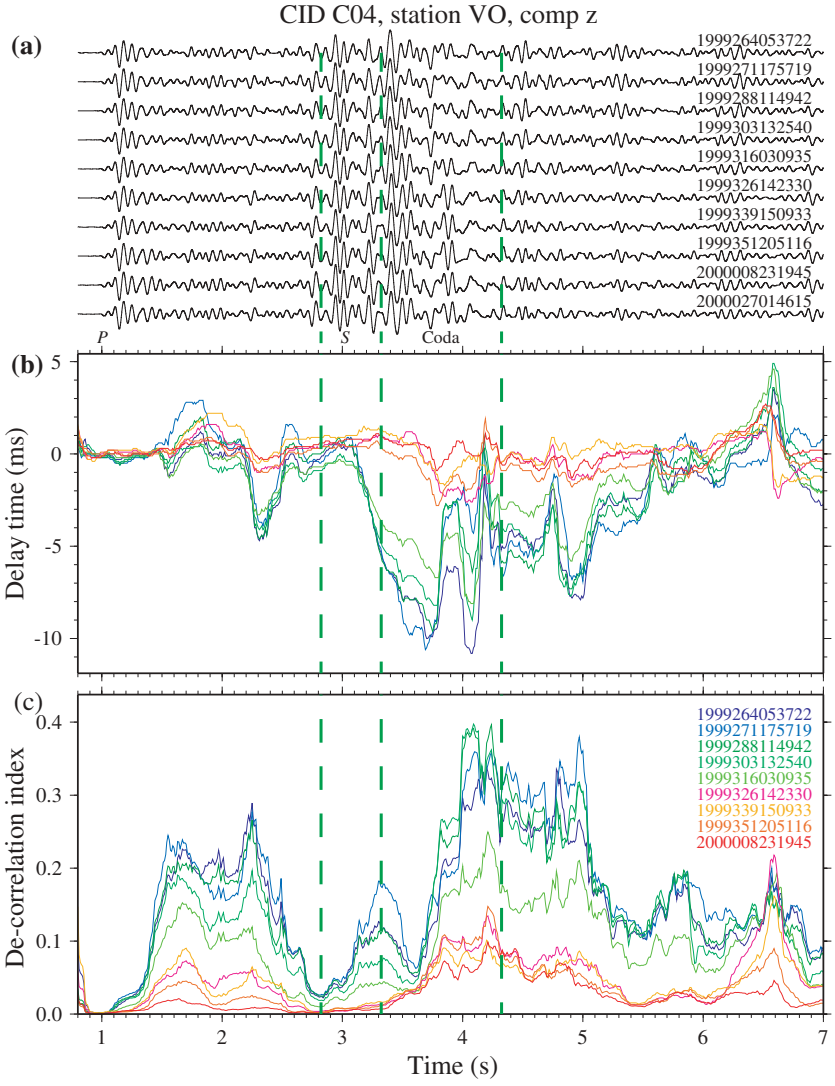

Figure 4

(a) Vertical-component seismograms generated by the 10 events in cluster C04 and recorded at station VO. Seismograms are aligned by *P* wave arrivals at 1 s. Calculated (b) delay time $\tau(t)$ and (c) decorrelation index $D(t)$. The vertical dashed lines denote the 1.0-s time window for the early *S*-coda waves, and the 0.5-s time window around the *S* arrival that are used to compute the median delay times. The event ID numbers are marked on the right side of panels (a) and (c), and consist of 4 digits year, 3-digits Julian day, 2-digits hour, 2-digits minute, and 2-digits seconds of the earthquake occurrence time.

median of $\tau(t)$ and $D(t)$ functions over a 1.0 s time window starting 0.3 s after the direct *S* arrival, and use these values in the later analysis. Slightly different time windows may result in different median values of $\tau(t)$ and $D(t)$. However, the general

patterns and overall conclusions that are based on statistics of hundreds of measurements remain essentially the same. To ensure the data quality, we keep only measurements that have a median $D(t)$ smaller than 0.3 and a signal-to-noise ratio larger than 3.

5. Results

5.1. Systematic Behavior of Temporal Changes in Delay Times

Figure 5 shows the median $\tau(t)$ and $D(t)$ values measured from the vertical-component seismograms for cluster C04 at 10 stations. The $\tau(t)$ values increase at the time of the Düzce main shock for all stations other than BV and CH, and the $D(t)$ values generally decrease. Since all the seismograms are compared with the last trace after the Düzce main shock, a decrease in $D(t)$ value (increase in correlation coefficient) is consistent with an increase in $\tau(t)$ value across the occurrence time of the Düzce main shock. Station VO that was installed inside the surface rupture zone of the İzmit earthquake has the largest coseismic change in median $\tau(t)$ and $D(t)$ values. Figure 6 displays the median $\tau(t)$ changes for 36 clusters at the fault zone station VO and a nearby station FP that is about 400 m from the İzmit rupture zone. The occurrence of the Düzce main shock produces distinct signals that are shown at both stations for 8 clusters along the Karadere segment (Figs. 6a,b), and 28 clusters around the Eften Lake area (Figs. 6c,d). However, the co-seismic changes at the fault zone station VO are about 50% larger than at station FP. We note that the median $\tau(t)$ values right after the Düzce main shock are larger for the 28 clusters around the Eften Lake area than those for the 8 clusters along the Karadere segment, possibly due to denser samplings of (larger) delays immediately following the main shock by the 28 clusters that are reactivated by the Düzce event. However, the temporal evolutions of delay times have similar shapes for different clusters with various source locations. This observation indicates that the temporal changes in $\tau(t)$ are most likely originated from the near-station structures, instead of the near-source regions or the propagation paths. We also note that, in some cases, changes with the same sense as those induced by the Düzce main shock begin before the Düzce event, and hence may be interpreted as precursory. However, these changes are associated with large scatter and require additional analysis that will be the subject of a future work.

Next, we merge the $\tau(t)$ measurements from the vertical-component seismograms of all clusters at each station (Fig. 7). Since our instruments worked in a trigger mode and most events are small, this results in a different number of recorded events at the different stations. In addition, only results with median $D(t)$ smaller than 0.3 and signal-to-noise ratio larger than 3 are kept. The final number of events and clusters analyzed for each station are indicated at the top of each panel in Figure 7. Most

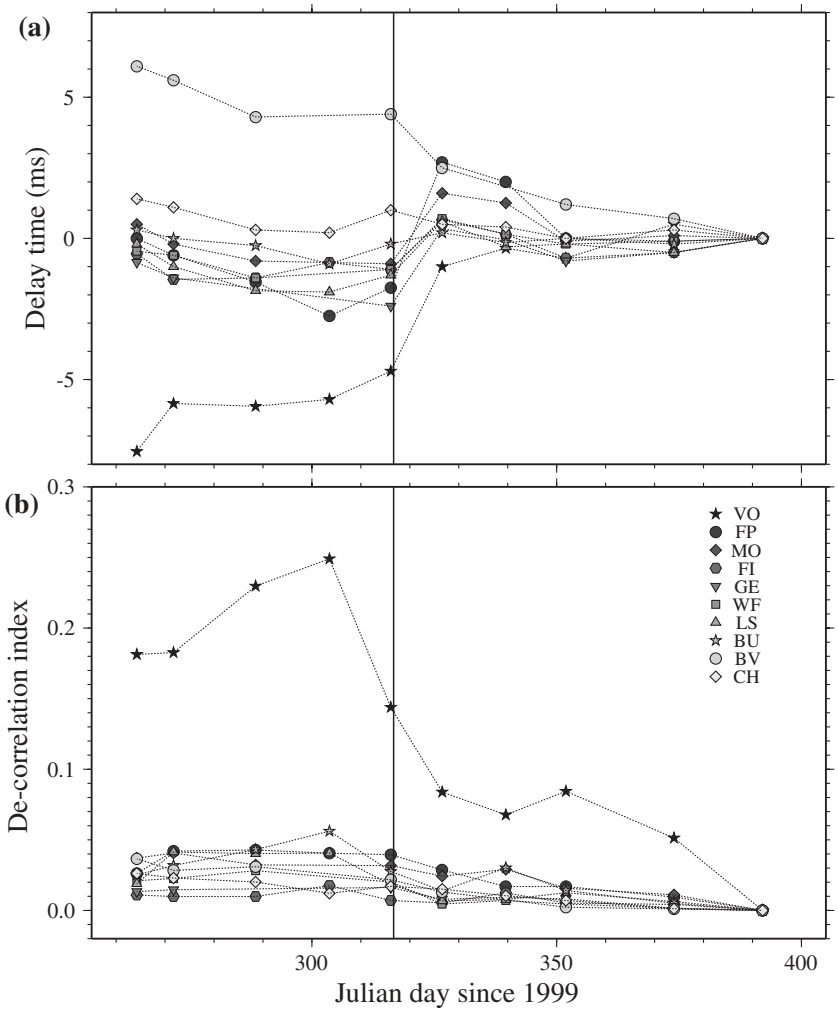

Figure 5
(a) Median delay time $\tau(t)$ and (b) decorrelation index $D(t)$ for the early *S*-coda waves plotted against the earthquake occurrence times for the vertical-component seismograms recorded at the 10 stations and generated by the earthquakes in cluster C04. The vertical line denotes the occurrence time of the Düzce main shock.

stations show clear increases in the median $\tau(t)$ values across the time of the Düzce main shock. An increase of $\tau(t)$ corresponds to a drop in the seismic velocity that is induced by the main shock. As noted before, the strength of the co-seismic increase of $\tau(t)$ is different among the 10 stations. In general, the fault zone station VO has the largest (up to 20 ms) co-seismic increase in $\tau(t)$ in the vertical component seismograms. The corresponding changes for stations FP, MO, FI, GE, WF, and

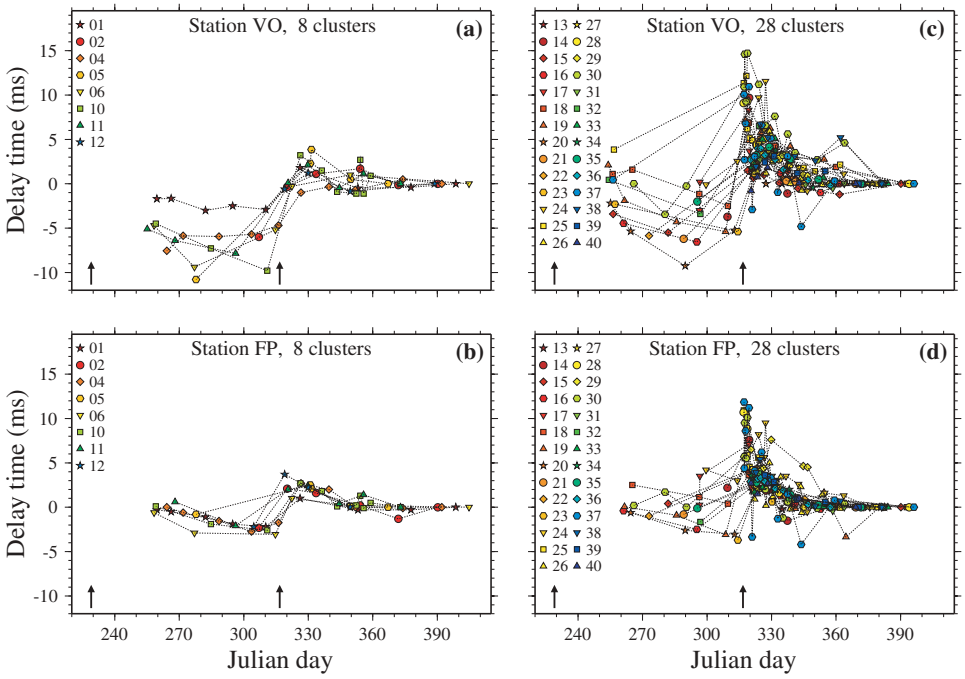

Figure 6

Median $\tau(t)$ for the early *S*-coda waves plotted against the earthquake occurrence times for the vertical-component seismograms recorded at stations VO (a) and FP (b) for 8 clusters along the Karadere segment. Median $\tau(t)$ values for 28 clusters around the Eften Lake area are shown in (c) and (d) for stations VO and FP, respectively. The $\tau(t)$ value for each cluster is denoted by a different symbol. The two vertical arrows mark the occurrence times of the İzmit and Düzce main shock.

LS are about 10–15 ms. Relatively small changes (around 5 ms) are observed for stations BU and BV, and station CH shows little or no observable co-seismic changes.

In addition to the clear co-seismic increases of delay times, we also observe that the $\tau(t)$ values for most stations gradually recover towards the levels that existed before the Düzce main shock (Fig. 8). This indicates that the rock damage heals (and the seismic velocity increases) in the post-main shock period. As shown in Figure 8, the decrease of $\tau(t)$ is approximately linear with logarithmic time. We fit the data by a least-squares procedure using a logarithmic relation

$$\tau(t) = a - b \log_{10}(t/\text{day}), \tag{3}$$

where a is the delay time in ms at 1 day after the main shock, b is a measure of the decreasing rate of the median $\tau(t)$ and $t/\text{day} \geq 0.1$. Because $\tau(t)$ diverges as t approaches 0 or infinity, this equation is valid for finite (relatively small) positive times. The threshold time of 0.1 day is chosen for all stations because it is about the

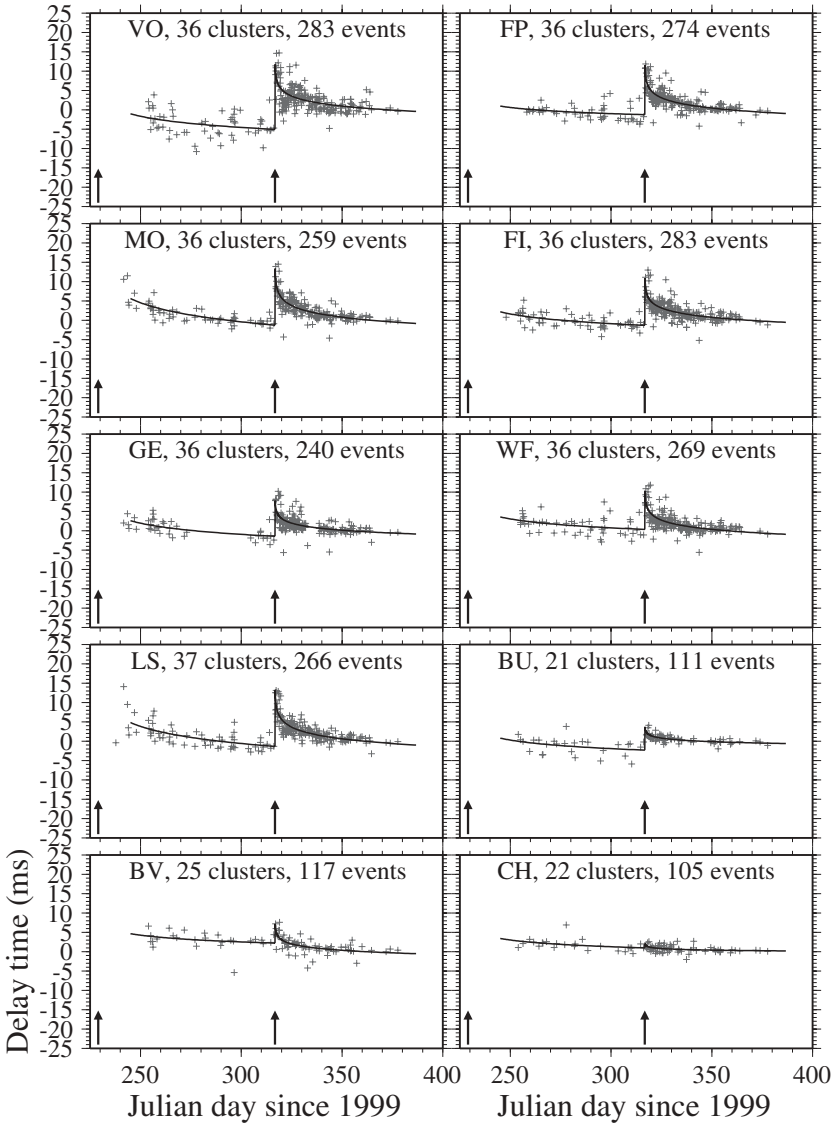

Figure 7

Median $\tau(t)$ for the early *S*-coda waves plotted against the earthquake occurrence times for the vertical-component seismograms recorded at the 10 stations. The two vertical arrows in each panel mark the occurrence times of the İzmit and Düzce main shock. The solid line in each panel denotes a least-squares fit to the data for each station using two logarithmic decay relations (Equation (3)) separately for the repeating events that occur between the İzmit and Düzce main shocks, and the events following the Düzce main shock.

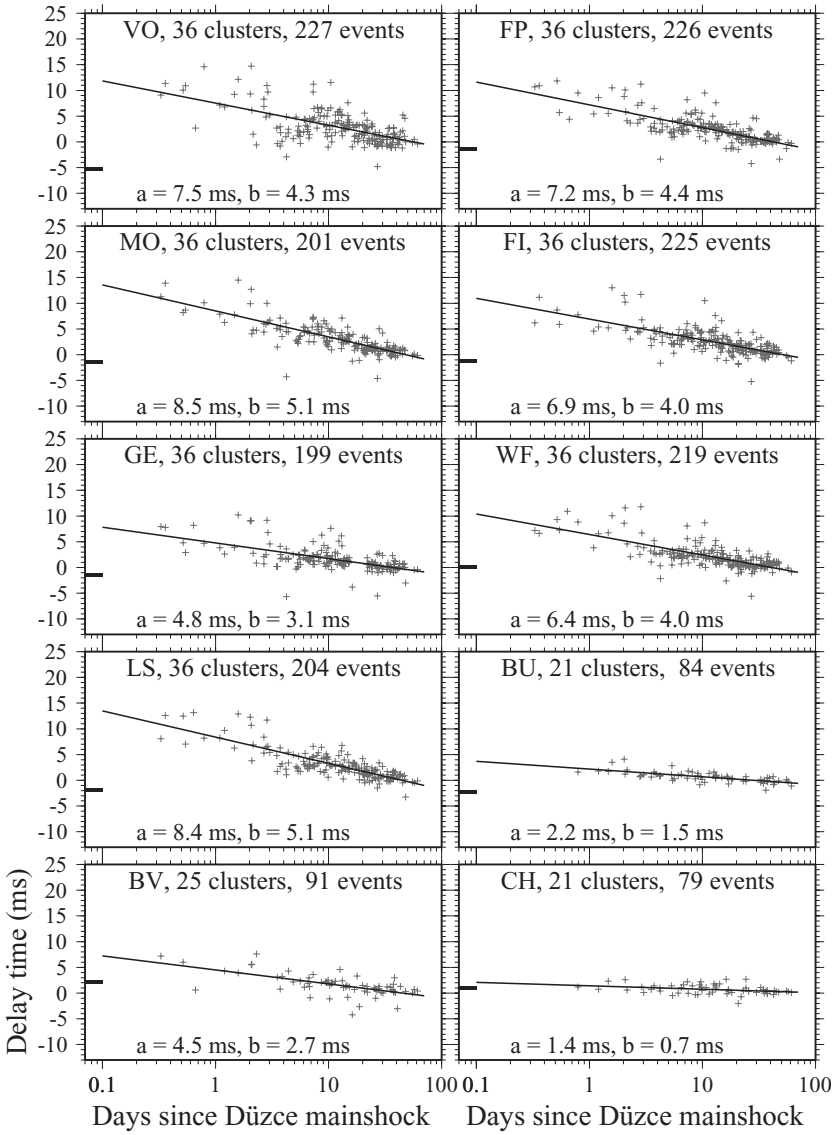

Figure 8

Median $\tau(t)$ for the early *S*-coda waves plotted against the logarithmic elapsed times after the Düzce main shock for the vertical-component seismograms recorded at the 10 stations. The solid line in each panel denotes a least-squares fit to the data for each station using the logarithmic decay relation (Equation (3)). The short horizontal bars on the left indicate the $\tau(t)$ levels before the Düzce main shock. The name of each station, total number of clusters and events for that station are marked at the top of each panel. The obtained values of a and b are indicated at the bottom of each panel.

earliest time when repeating earthquakes identified in this study start after the Düzce main shock. The parameter a is associated with initial conditions, while the parameter b represents a healing rate. For example, in the damage rheology model of LYAKHOVSKY *et al.* (1997, 2005), the fitting parameters a and b correspond, respectively, to the initial damage level and the damage healing rate. The obtained values of a and b for the time period following the Düzce main shock are indicated in the panels of Figure 8. After three months, the delays for most stations return close to the levels that existed before the Düzce main shock. However, this does not hold for the fault zone station VO which experienced the largest co-seismic change and is likely to have longer recovery time and larger permanent deformation than the other stations.

Since our temporary network straddled the rupture zones of both the İzmit and Düzce main shocks, it recorded many clusters that were activated right after the İzmit main shock. These clusters can be used to obtain information on the temporal changes associated with the İzmit event. Unfortunately, the network was deployed one week after the İzmit main shock and some stations that were installed in the first two weeks were later removed. Thus, we cannot constrain the temporal changes in the co- and early post-seismic period of the İzmit event. However, most stations show a gradual decrease in $\tau(t)$ after the İzmit main shock that is similar to the healing process observed more clearly after the Düzce main shock (Fig. 8). As shown in Figure 7, the healing process after the İzmit event was interrupted abruptly by the occurrence of the Düzce main shock three month later. Similar patterns have been observed for the M7.3 1992 Landers and M7.1 1999 Hector Mine earthquakes (VIDALE and LI, 2003), and for the M6.9 1989 Loma Prieta earthquake and its largest aftershock, the M5.4 1990 Chittenden earthquake (RUBINSTEIN and BEROZA, 2004b).

We use the same logarithmic functional form (Equation (3)) to fit the data observed between the İzmit and Düzce main shocks, as well as after the Düzce main shock. Due to lack of data in the early post-İzmit period, the parameters a and b are probably not well constrained for that period. Nevertheless, the procedure allows us to estimate the level of delay time right before the Düzce main shock, and the co-seismic increase in delay time at each station associated with the Düzce event. Specifically, the pre-Düzce-main shock level is evaluated using the fitting parameters obtained for the post-İzmit data at the time of the Düzce main shock. The level of delay time right after the Düzce main shock is computed at 0.1 day after the main shock using the fitting parameters obtained for the post-Düzce data. The differences between the pre- and post-Düzce levels represent the co-seismic increases in delay times at the various stations (Table 1).

Similar patterns of median $\tau(t)$ values for the early S-coda waves are shown, with larger amplitudes, for the north component seismograms at each station (Fig. 9), indicating that our observations are robust. Analysis of the east components produces very similar patterns to those associated with the north components. These results are not shown in a separate figure but are included in a later summary

Table 1

Station parameters, observed co-seismic delays, and peak ground accelerations during the Düzce main shock

Station	Latitude	Longitude	Distance to rupture (km)	Co-seismic delays (ms)			PGA (g)		
				Z	N	E	Z	N	E
VO	40.7429	30.8761	0.00	16.81	30.65	26.67	0.20	0.89	0.56
FP	40.7448	30.8720	0.41	12.83	17.41	17.88	0.10	0.15	0.14
MO	40.7267	30.8220	0.00	14.63	15.54	15.05	N/A	N/A	N/A
FI	40.7229	30.8220	0.34	12.29	14.55	17.08	0.10	0.14	0.27
GE	40.7448	30.8720	4.86	9.23	7.67	9.16	N/A	N/A	N/A
WF	40.7025	30.8553	3.49	9.99	13.73	15.24	0.06	0.16	0.12
LS	40.7201	30.7922	0.00	14.62	19.92	21.90	0.05	0.10	0.13
BU	40.7774	30.6128	11.34	6.00	8.47	9.02	0.02	0.03	0.05
BV	40.7552	31.0149	1.00	5.00	6.72	4.21	0.07	0.08	0.11
CH	40.6698	30.6655	1.42	1.12	7.04	6.82	0.02	0.03	0.05

Station VO, MO, and LS are inside the surface rupture of the İzmit earthquake. Station BV is about 1 km from a 2 m scarp formed during the Düzce earthquake (SEEBER *et al.*, 2000). Station FP is about 410 m from fault zone station VO. Station FI is about 340 m from fault zone station MO. The distances to the Karadere segment for the remaining stations (GE, WF, and CH) are computed by projecting to a line that is centered at station MO with a strike of 70°.

Figures 11 and 13. We note that the observed co-seismic changes for the horizontal components are larger than those of the vertical component (Figs. 7, 9; Table 1). This is probably because the horizontal seismograms contain more (and hence are more sensitive to changes of) *S*-wave energy than the vertical seismograms. In addition, the horizontal seismograms are more sensitive to site amplifications and other local near-station structures than the vertical ones (e.g., CASTRO *et al.*, 1997). As illustrated in Figure 4, we also measure changes in delay time for the direct *S* arrival using the median of $\tau(t)$ with a 0.5 s window starting 0.2 s before the picked *S* arrival. A summary of results associated with such analysis of the direct *S* waves is given in Figure 10. The patterns are similar to those observed for the early *S*-coda waves (Fig. 7), although the amplitudes in Figure 10 for the direct *S* waves are smaller that those associated with the *S*-coda waves.

Figure 11a gives the healing rates following the Düzce main shock based on analysis of all three components of motion at the ten different stations versus the corresponding co-Düzce time delays. Figure 11b plots the post-Düzce healing rates at all stations and components of motion versus the corresponding post-İzmit healing rates. The results of Figure 11a show that the post-Düzce healing rates are strongly correlated with the co-seismic delays. This indicates that the function that governs the recovery process is nonlinear, i.e., the healing rate depends strongly on the damage level, as in the damage model of LYAKHOVSKY *et al.* (1997, 2005). For most stations, a similar time interval of about three months is needed for near-complete post-Düzce recovery. The results at the fault zone station VO deviate from

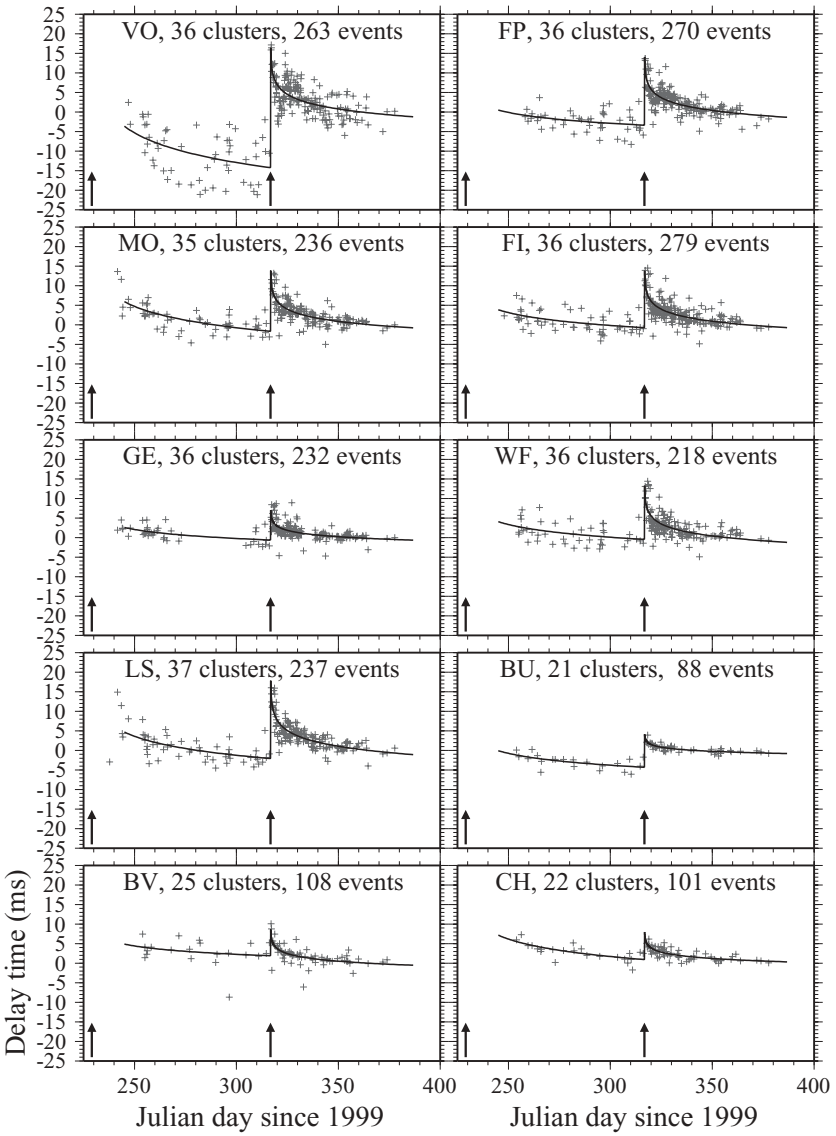

Figure 9
Median $\tau(t)$ for the early *S*-coda waves plotted against the earthquake occurrence times for the north-component seismograms recorded at the 10 stations. Other symbols and notations are the same in Figure 7.

this trend and indicate, as mentioned before, a longer recovery process and possible larger permanent change. The results of Figure 11b show that the post-Düzce healing rates correlate well with, and are about half of, the post-İzmit healing rate. Since the

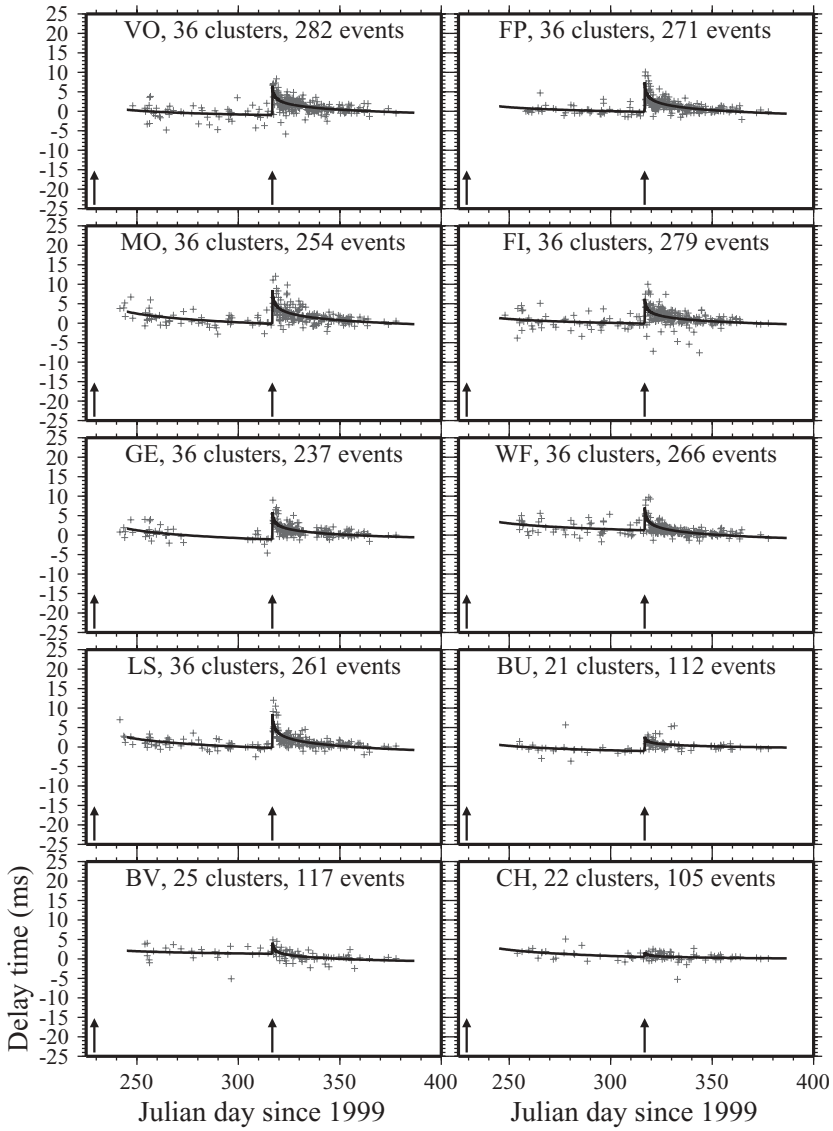

Figure 10
Median $\tau(t)$ for the S waves plotted against the earthquake occurrence times for the vertical-component seismograms recorded at the 10 stations. Other symbols and notations are the same in Figure 7.

healing rates depend strongly on the co-seismic delays, this suggests that the co-seismic delays for the İzmit main shock could be twice as large as those generated by the Düzce main shock.

The observed correlations lend support to the robustness of the measurements and indicate that the results reflect characteristics of the various sites. As will be

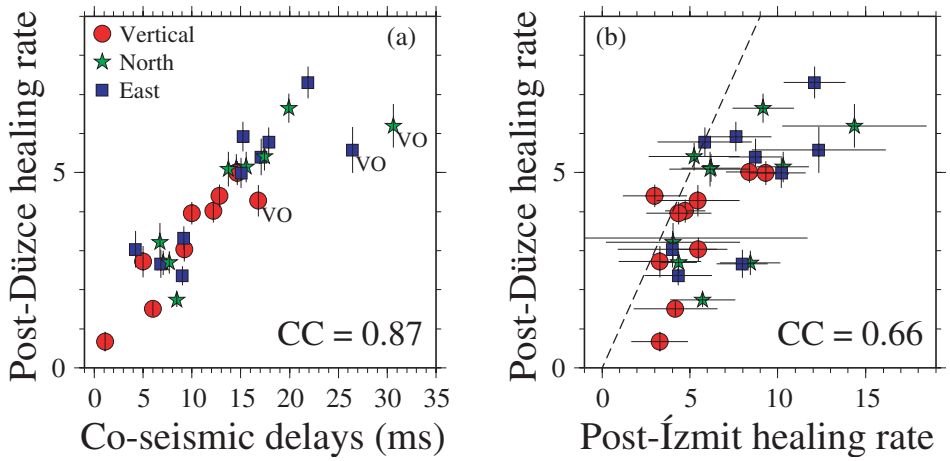

Figure 11
(a) The healing rates (ms per decade change in time) after the Düzce main shock plotted versus the co-seismic delays (ms) for all three components of motions at the 10 stations. Red circles, green stars, and blue squares denote results for the vertical, north, and east components, respectively. The bar on top of each symbol marks the standard error of each measurement. The correlation coefficient (CC) between the two values is marked in the bottom right of the figure. The results for station VO are marked by its station name. (b) The healing rates after the Düzce main shock plotted versus the healing rates after the İzmit main shock. The dashed line denotes a 1-1 relationship.

discussed below, the co-seismic delays strongly depend on the peak ground acceleration generated by the Düzce main shock. Since the İzmit event had about three times as large moment release as the Düzce event, it is plausible that the damage levels created during the İzmit main shock are twice as large as those generated during the Düzce main shock. However, the lack of recordings during the co-seismic and early post-seismic period of the İzmit main shock prevents us from reaching more definitive conclusions.

5.2. Possible Regions of Temporal Changes

The observed temporal evolution of $\tau(t)$ in the *S*-coda waves can be caused by systematic shifts in the hypocentral locations, and/or temporal changes of material properties near the source regions, along the source-receiver paths, or near the receivers. In this section, we attempt to constrain the factors that contribute to the observed temporal changes.

It has been noted that up to 0.1 s delay changes in later *S*-coda waves can be solely generated by event separation over a distance of about 500 m (Got and Coutant, 1997). However, it is unlikely that our observed temporal changes of $\tau(t)$ are caused mainly by changes in source locations. This is because the detailed relocation analysis discussed in section 2.2 enables us to collocate the employed events in each cluster to $\sim$10 m precision (Fig. 2), thereby removing most of the

effects from source shifts. In addition, we found that temporal changes for clusters having considerably different locations are similar to each other at a given station (Fig. 6). This indicates again that source shifts are not the primary cause for the observed temporal changes. The same observation can be used to rule out velocity changes near the source regions as the primary cause. We also observe (Fig. 5) that temporal changes of waveforms in a given cluster are not the same at nearby stations (e.g., stations VO and FP). If the contributions to $\tau(t)$ come mostly from the source regions, we would expect to see the opposite. Thus, neither shifts in hypocentral locations nor near-source velocity changes are the dominant causes of the observed $\tau(t)$ in the *S*-coda waves.

It is difficult to constrain the precise fractions of changes contributed by source-receiver path and near-station site effects. The most likely candidate regions that produce the observed $\tau(t)$ are the heavily-damaged top few hundred meters of the crust and the recently ruptured fault zone sections. If the seismic velocities were reduced over much of the seismogenic zone, we would expect to observe the largest $\tau(t)$ at the most distant stations. However, the most distant station BU has the smallest $\tau(t)$ among all stations. Station BV is very close to the rupture zone of the Düzce main shock and right above the clusters around the Eften Lake. However, the $\tau(t)$ values at station BV are the second smallest among all stations. The observed changes of $\tau(t)$ are largest at the fault zone stations VO, MO, and LS; however, the changes do not increase with increasing propagation distance along the rupture zone (Fig. 5). We also observe that stations GE and WF that are clearly outside the fault zone have significant delays.

We have shown that the temporal changes are similar at most stations for clusters with quite different source locations (Fig. 6). We also observe clear differences in the strength of the co-seismic increase in $\tau(t)$ for stations that are close to each other. For example, station VO that was deployed inside the surface rupture zone of the İzmit earthquake along the Karadere segment has the largest (up to 30 ms, Table 1) co-seismic increase in $\tau(t)$. The changes for station FP $\sim$400 m away from station VO are somewhat smaller, on the order of 10–20 ms. Finally, we found that the post-Düzce healing rate correlates well with the post-İzmit healing rate, suggesting that the responses at a given site to the two main shocks are similar. The results indicate that most of the temporal changes are associated with shallow site effects that are largest for the fault zone stations.

5.3. Relations of Temporal Changes and Düzce Main shock Ground Motion

In section 5.2, we have argued that the near-station structure plays a dominant role in the observed temporal delays in the early *S*-coda waves. Here we show that the ground motion generated by the seismic waves radiated from the Düzce main shock are most likely the cause of the observed co-seismic changes of delay times. All stations other than MO and GE had three-component FBAs, collocated with the L22

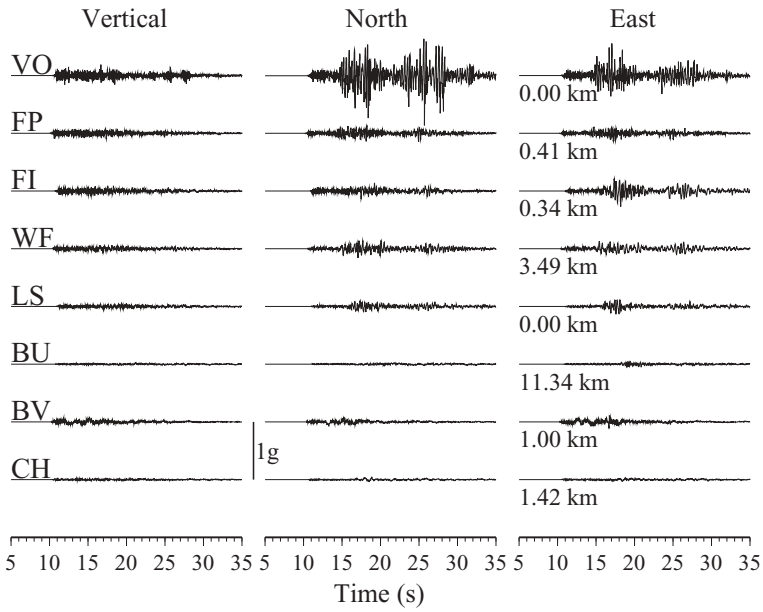

Figure 12
Three-component strong ground motion seismograms for the Düzce main shock recorded at 8 stations (not including MO and GE). All seismograms are plotted using a fixed scale of 1 g. The value under each east-component seismogram denotes the normal distance of each station to the recently ruptured fault zone.

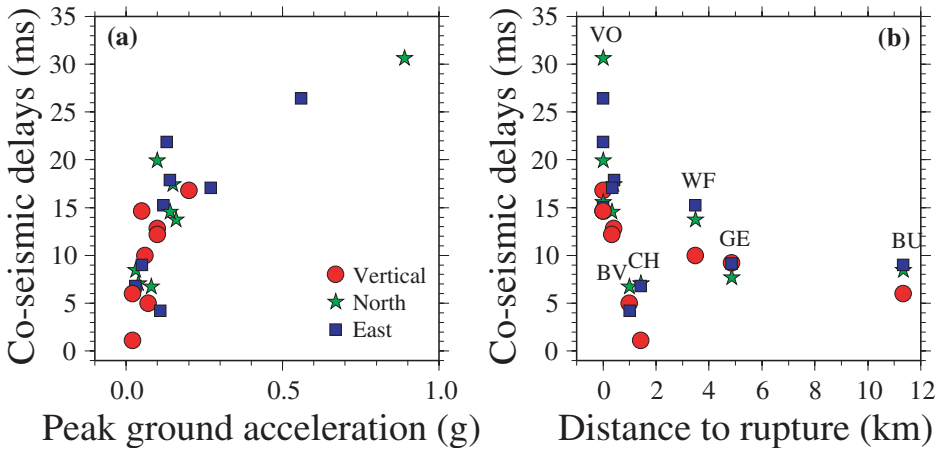

Figure 13
(a) The co-seismic delays plotted against the peak ground accelerations for eight stations (not including MO and GE). Red circles, green stars, and blue squares denote results for the vertical, north, and east components, respectively. (b) The co-seismic delays plotted versus the normal distances to the recently ruptured fault zone for the 10 stations. The results for stations VO, BV, CH, WF, GE, and BU are marked by their station names on the top of the corresponding symbols.

short-period sensors, that recorded strong ground motions generated by the M_w7.1 Düzce main shock (Fig. 12). The peak ground acceleration (PGA) parameters at the different stations are listed in Table 1. Figure 13a compares the PGA values with the observed co-seismic delays in the early *S*-coda waves. The results show a clear correlation between the observed delays and observed PGA values. Similar correlations were observed around the 1989 Loma Prieta earthquake (RUBINSTEIN and BEROZA, 2004a,b) and the 2004 Parkfield earthquake (RUBINSTEIN and BEROZA, 2005).

Figure 13b plots the co-seismic delay caused by the Düzce main shock at each station against its normal distance from the recently ruptured fault trace (D_r). Except for station BV which is close to the rupture zone of the Düzce main shock, the D_r values for the other nine stations are measured against the Karadere segment that ruptured during the İzmit earthquake. The co-seismic delays show an inverse correlation with the D_r values, except for stations BV and CH. A comparison of the results in Figures 13a and 13b indicates that the PGA values, observed time delays, and D_r values, all are generally correlated. Station VO which is inside the Karadere segment recorded up to 0.9 g during the Düzce main shock, and has up to 30 ms co-seismic delays. In comparison, peak accelerations recorded at station FP $\sim$400 m away from station VO is 0.16 g and the largest co-seismic delay there is $\sim$18 ms. However, station BV that is close to the western terminus of the Düzce rupture zone recorded only 0.1 g during the Düzce main shock and has small co-seismic delays. These low values suggest that station BV is probably located on a competent rock site near the end of the Düzce rupture zone. This is consistent with the relatively low triggers at that station during the experiment (SEEBER *et al.*, 2000). Stations MO and LS which are inside the Karadere segment have similar ground motions and co-seismic delays to those at nearby stations FI, GE, and WF. The small PGA and co-seismic delays at station CH could be explained by the relatively large distance from the Düzce epicenter. The different responses in fault zone stations VO, MO and LS indicate strong variations of motion amplification along the strike of the fault.

6. Discussion and Conclusions

We constructed a data set consisting of 36 clusters of highly repeating earthquakes in the aftershock zones of the 1999 M_w7.4 İzmit and M_w7.1 Düzce earthquakes. The decay rates of repeating events in individual clusters following the Düzce main shock are compatible with the $1/t$ Omori law for aftershock decay rates (OMORI, 1895), although other functions can also fit the limited available data (e.g., KISSLINGER, 1996; BEN-ZION and LYAKHOVSKY, 2006). Using waveforms generated by the repeating earthquake clusters, we identified systematic changes in travel times of the *S* and early *S*-coda waves relative to the *P* waves. We interpret the travel-time changes as temporal variations of seismic velocity in the shallow crust around the

Karadere-Düzce branch of the NAF that ruptured during the two main shocks. The co-seismic delay times at the various stations correlate well with the corresponding strong ground motions recorded during the Düzce main shock, indicating that shaking-induced damage is the most likely mechanism for the observed temporal changes. The amplitudes of delay times after the Düzce main shock follow a logarithmic decay, showing a post-main shock recovery of the shallow rock damage. Our results are compatible with recent observations of abrupt velocity reductions followed by post-seismic recoveries associated with several medium to large ($M > 5$) earthquakes, including the Loma Prieta earthquake and its largest aftershock (RUBINSTEIN and BEROZA, 2004a,b), the Morgan Hill earthquake (SCHAFF and BEROZA, 2004), the Hector Mine earthquake (VIDALE and LI, 2003), and the 2004 Parkfield earthquake (RUBINSTEIN and BEROZA, 2005).

The largest co-seismic velocity decrease is observed at station VO that was deployed inside the rupture zone of the 1999 İzmit earthquake and recorded $\sim$0.9 g ground acceleration during the Düzce main shock. The observed co-seismic changes and ground motions generated by the Düzce main shock at the different stations generally decrease with normal distance from the rupture zone. As summarized by BEN-ZION and SAMMIS (2003), large fault zones are characterized by zones of damaged rock with intense microcracks and lower seismic velocity than the surrounding rocks. Such zones are expected to produce large motion amplification (BEN-ZION and AKI, 1990), as observed here and the studies of CORMIER and SPUDICH (1984), SPUDICH and OLSEN (2001), SEEBER *et al.* (2000), and ROVELLI *et al.* (2002). Recent systematic analyses of fault zone trapped waves (e.g., BEN-ZION *et al.*, 2003; PENG *et al.*, 2003; LEWIS *et al.*, 2005) and near-fault crustal anisotropy (e.g., COCHRAN *et al.*, 2003; BONESS and ZOBACK, 2004; PENG and BEN-ZION, 2004; LIU *et al.*, 2004) associated with several large earthquakes (including the İzmit and Düzce events) showed that the belts of damaged fault zone rock are confined primarily to the top 3–4 km of the crust. Seismic waves generated by sources outside such shallow low velocity fault zone layers can be significantly amplified inside the damaged fault zone layers (e.g., BEN-ZION *et al.*, 2003; FOHRMANN *et al.*, 2004). Owing to the nonlinearity of damage evolution (e.g., LYAKHOVSKY *et al.*, 1997), it is easier to produce additional damage in a rock volume that is already damaged. The above factors contribute to the observed large ground motions and co-seismic delays at the fault zone stations. Our results also show strong variations of fault zone amplification along strike, compatible with our previous analyses of fault zone trapped waves and anisotropy.

The observation that stations clearly outside the fault zone also have clear changes in delay times implies that the rock damage induced by the İzmit and Düzce main shocks is not limited to the immediate vicinity of the fault zone. The co-seismic and post-main shock patterns generated by repeating earthquake clusters of different depth are very similar, indicating that the changes of material properties occur in the shallow crust. The observation of similar patterns following the occurrence of smaller

earthquakes (RUBINSTEIN and BEROZA, 2004a,b, 2005) suggest strongly that the damage occurred in the very shallow, heavily damaged, surface layer of the crust.

While our observations and other studies suggest that the dominant changes occur near stations and are likely to be shallow, we do not rule out small temporal changes near the source or along the propagation path. The 8 clusters along the Karadere segment and the 28 clusters around the Eften Lake in Figure 6 exhibit similar trends in delays; however, there are slight variations in the results. Although most of the variations may be explained by the differences in occurrence times that are modulated by the Düzce main shock, the co-seismic delays and decay rates after the Düzce main shock for the 8 clusters along the Karadere segment appear to be smaller than those associated with the 28 clusters around the Eften Lake. Since the latter 28 clusters around the Eften Lake are located on the north-dipping faults that failed during the Düzce main shock, the difference may include changes near the source or along the propagation path. However, the delays at station BV that is within 1 km of the Düzce rupture zone are very small for all clusters and we do not find systematic relations between the delays and the hypocentral depths of the clusters. These observations indicate that changes near the stations play the dominant role in explaining the general behavior of the time-dependent effects in our data.

Some properties of the regions generating the time-dependent effects may be inferred by examining the relation between the portions of the seismograms showing the largest effects and a clear reference phase like the direct *S* arrival. In the example of Figure 4, the largest delays are observed in the early *S*-coda waves and similar results were obtained by NIU *et al.* (2003) for the Parkfield segment of the San Andreas fault. SCHAFF and BEROZA (2004) found that the delays are peaked at around 2–3 s after the *S* arrival and then drop back for the aftershock zone of the Loma Prieta earthquake. We performed a systematic check for all 36 clusters at all 10 stations, but did not find any clear relation between the largest delays and the times after the *S* arrival. We speculate that although the velocity reductions occur mostly near the surface, the distribution of the regions generating the changes is not uniform. As indicated before, regions with higher initial damage are expected to produce larger time-dependent effects. It is likely that the fault zone stations (especially VO) pick some changes associated with the fault zone layer producing trapped waves, but the observed temporal changes are widespread and indicate overall a shallow regional origin associated with a near-surface layer.

Laboratory studies have shown that rocks, soils, and other granular materials exhibit universal nonlinear characteristics in response to dynamic deformation (e.g., JOHNSON and SUTIN, 2005). These characteristics include a decrease in elastic modulus or wave speed and increased dissipation with increasing input strain, which are generally termed ''nonlinear fast dynamics'' (NFD). Another important behavior termed ''slow dynamics'' (SD) is a logarithmic recovery of material properties over 10^3–10^4 s after dynamic excitation (e.g., TEN CATE and SHANKLAND, 1996; TEN CATE

et al., 2000). In the last 15 years, wide-spread nonlinear strong ground motion effects were reported at sediment sites (e.g., CHIN and AKI, 1991; FIELD *et al.*, 1997; AGUIRRE and IRIKURA, 1997; PAVLENKO and IRIKURA, 2002, 2003; BOUCHON *et al.*, 2004). The validity of some of those observations has been questioned by WENNERBERG (1996) and O'CONNELL (1999). Our observations of co-seismic changes of seismic velocities followed by logarithmic recovery, along with those others (VIDALE and LI, 2003; SCHAFF and BEROZA, 2004; RUBINSTEIN and BEROZA, 2004a,b), provide additional support that nonlinearity is wide-spread in the shallow crust during strong ground motion of moderate to large earthquakes. However, it is important to note that the time scale of the logarithmic recovery observed in the above lab studies is on the order of hours to days, rather than the months to years scales associated with this and other field studies. Longer recovery times than those observed in the dynamic deformation experiments are implied by the quasi-static experiments associated with rate- and state-dependent friction (e.g., DIETERICH, 1978; BEELER *et al.*, 1994; DIETERICH and KILGORE, 1996; MARONE, 1998). The differences in the recovery time scales probably reflect differences in the mechanisms operating during the dynamically-driven lab experiments, quasi-static lab experiments, and the yet slower quasi-static process in the field, as well as (potentially large) differences in the initial damage and frequency content of the waves.

Because the earliest repeating earthquakes that were used in this study were at least 0.1 days (2.4 hours) after the Düzce main shock, the co-seismic delays were estimated from the differences between pre-Düzce delay times and post-Düzce delay times at 0.1 day after the main shock. Since the changes follow a logarithmic recovery with time, we expect larger changes in time right after the main shock than those in latter times. Thus, the obtained co-seismic delays in this study are lower bounds. A systematic search for repeating earthquakes in the early aftershock period (e.g., PENG and VIDALE, 2004) could provide useful information on the co-seismic changes in material properties of the shallow crust, and how they evolve within the initial minutes to hours after strong shaking. However, it is extremely difficult to obtain reliable measurements in the noisy coda waves generated by main shocks and large aftershocks.

In a previous analysis of shear-wave splitting using the same data set (PENG and BEN-ZION, 2005), we found only small (2% or less) co-seismic changes of anisotropy parameters at the time of the Düzce main shock, and no appreciable post-main shock recoveries (or pre-main shock precursory evolution). In this study we found clear travel-time changes in *S* and early *S*-coda waves (up to 30 ms). The obtained values correspond to fractional slowness (inverse of velocity) changes of up to 3%, assuming that the decay is accumulated within the 1-s early *S*-coda waves window. This is similar to the values obtained in other studies (e.g., VIDALE and LI, 2003; SCHAFF and BEROZA, 2004). We cannot compare directly the percentage of changes obtained from the earlier shear-wave splitting analysis (PENG and BEN-ZION, 2005) and the early *S*-coda waves of this study. However, it is clear that measuring travel-

time changes in coda waves by the sliding window waveform cross-correlation technique generally provides a better way of detecting possible temporal changes than analysis of shear-wave splitting. This is probably because of the following three reasons. First, shear-wave splitting is sensitive to a dominant subset of cracks with given orientation, whereas coda waves are sensitive to the entire crack population. Second, shear-wave splitting delay times are obtained from the direct *S* waves, which are typically less sensitive to possible temporal changes in the medium than the *S*-coda waves with longer travel time and propagation distance (e.g., SNIEDER, 2006). Third, standard shear-wave splitting analysis typically requires clear *S* waves that are recorded on three-component instruments, similar wave forms between fast and slow *S* waves, and earthquake sources within the shear-wave window (NUTTLI, 1961). Sometimes strict criteria are applied to obtain a ''high quality'' shear-wave splitting measurement (e.g., MATCHAM *et al.*, 2000; PENG and BEN-ZION, 2004, 2005). These requirements prevent many seismograms from being used in the anisotropy analysis. On the other hand, the sliding window waveform cross-correlation technique can be applied to single-component seismograms only (e.g., SCHAFF and BEROZA, 2004), and for earthquakes at various distances from the recording stations. Thus, although shear-wave splitting is a useful tool for analyzing structural anisotropy in the crust and upper mantle (e.g., LEARY *et al.*, 1990; SILVER, 1996; SAVAGE, 1999, and references therein), it appears that measuring travel-time changes in the *S*-coda waves has significant advantages over shear-wave splitting analysis in terms of identifying temporal changes of crustal properties.

We note that the observations discussed in this work and our previous studies on the north Anatolian fault and other large faults and rupture zones (BEN-ZION *et al.*, 2003; PENG *et al.*, 2003; LIU *et al.*, 2004, 2005; PENG and BEN-ZION, 2004, 2005; LEWIS *et al.*, 2005), as well as other related works based on trapped waves, anisotropy and coda waves (e.g., VIDALE and LI, 2003; SCHAFF and BEROZA, 2004; RUBINSTEIN and BEROZA, 2004a,b) reflect only properties of the shallow (e.g., $\sim$3–4 km) or very shallow (e.g., $\sim$200 m) top sections of the crust. Imaging the key mechanical structure of faults at seismogenic depths, where earthquakes nucleate and the bulk of co-seismic slip occurs, remains a significant observational challenge. Fault zone head waves refracting along material discontinuity interfaces in the structure of large faults provide a promising approach for resolving important fault zone properties throughout the seismogenic zone (BEN-ZION *et al.*, 1992; MCGUIRE and BEN-ZION, 2005).

Acknowledgments

We are grateful to John Armbruster, David Okaya, Naside Ozer and Nano Seeber for essential help with the fieldwork, and to PASSCAL for providing the equipment and technical support for the experiment. We thank Fenglin Niu for

sharing his sliding window cross-correlation code, and Elizabeth Cochran, Joan Gomberg, Yunfeng Liu, and Paul Silver for useful discussions. The manuscript benefited from valuable comments by referees Justin Rubinstein and Roel Snieder and Editor Willie Lee. All figures were generated using GMT (WESSEL and SMITH, 1998). The study was supported by the National Science Foundation (Grant EAR0003401).

REFERENCES

AGUIRRE, J. and IRIKURA, K. (1997), *Nonlinearity, liquefaction, and velocity variation of soft soil layers in Port Island, Kobe, during the Hyogoken-Nanbu earthquake*, Bull. Seismol. Soc. Am. *87*, 1244–1258.

AKI, K. (1985), *Theory of earthquake prediction with special reference to monitoring of the quality factor of lithosphere by the coda method*, Earthq. Pred. Res. *3*, 219–230.

AKI, K. and CHOUET, L.B. (1975), *Origin of coda waves: Source, attenuation, and scattering effects*, J. Geophys. Res. *80*, 3322–3342.

ANTOLIK, M., NADEAU, R.M., ASTER, R.C., and MCEVILLY, T.V. (1996), *Differential analysis of coda Q using similar microearthquakes in seismic gaps, Part 2: Application to seismograms recorded by the Parkfield High Resolution Seismic Network*, Bull. Seismol. Soc. Am. *86*, 890–910.

ASTER, R.C., SHEARER, P.M., and BERGER, J. (1990), *Quantitative measurements of shear-wave polarizations at the Anza seismic network, southern California: Implications for shear-wave splitting and earthquake prediction*, J. Geophys. Res. *95*, 12449–12473.

ASTER, R.C., SHEARER, P.M., and BERGER, J. (1991), *Comments on Quantitative measurements of shear-wave polarization at the Anza seismic network, Southern California: implications for shear-wave splitting and earthquake prediction by ASTER, R.C., Shearer, P.M. and Berger J. – Reply*, J. Geophys. Res. *96*, 6415–6419.

BEELER, N., TULLIS T.E., and WEEKS, J.D. (1994), *The roles of time and displacement in the evolution effect in rock friction*, Geophys. Res. Lett. *21*, 1987–1990.

BEN-ZION, Y., *Appendix 2. Key formulas in earthquake seismology*. In *The IASPEI International Handbook of Earthquake and Engineering Seismology, Part B* (eds. Lee, W.H.K., Kanamori, H., Jennings, P.C., and Kisslinger C.) (Academic Press, London 2003) pp. 1857–1875.

BEN-ZION, Y. and AKI, K. (1990), *Seismic radiation from an SH line source in a laterally heterogeneous planar fault zone*, Bull. Seismol. Soc. Am. *80*, 971–994.

BEN-ZION, Y., KATZ, S., and LEARY, P. (1992), *Joint inversion of fault zone head waves and direct P arrivals for crustal structure near major faults*, J. Geophys. Res. *97*, 1943–1951.

BEN-ZION, Y. and LYAKHOVSKY, V. (2006), *Analysis of aftershocks in a lithospheric model with seismogenic zone governed by damage rheology*, Geophys. J. Int., 164, doi: 10.1111/j.1365-246x.2006.02878.x.

BEN-ZION, Y., PENG, Z., OKAYA, D., SEEBER, L., ARMBRUSTER, J.G., OZER, N., MICHAEL, A.J., BARIS, S., and AKTAR, M. (2003), *A shallow fault zone structure illuminated by trapped waves in the Karadere-Düzce branch of the north Anatolian Fault, western Turkey*, Geophys. J. Int. *152*, 699–717.

BEN-ZION, Y. and SAMMIS, C.G. (2003), *Characterization of fault zones*, Pure Appl. Geophys. *160*, 677–715.

BEN-ZION, Y. and ZHU, L. (2002), *Potency-magnitude scaling relations for southern California earthquakes with* $1.0 < M_L < 7.0$, Geophys. J. Int. *148*, F1–F5.

BEROZA, G.C., COLE, A.T., and ELLSWORTH, W.L. (1995), *Stability of coda wave attenuation during the Loma Prieta, California, earthquake sequence*, J. Geophys. Res. *100*, 3977–3987.

BOKELMANN, G.H.R. and HARJES, H.P. (2000), *Evidence for temporal variation of seismic velocity within the upper continental crust*, J. Geophys. Res. *105*, 23879–23894.

BONESS, N.L. and ZOBACK, M.D. (2004), *Stress-induced seismic velocity anisotropy and physical properties in the SAFOD Pilot Hole in Parkfield, CA*, Geophys. Res. Lett. *31*, L15S17, doi:10.1029/2004GL019020.

BOUCHON, M., KARABULUT, H., DIETRICH, M., BOUIN, M., and AKTAR, M. (2004), *Effect of fault zone on strong ground motion*, EOS Trans. AGU *85(47)*, Fall Meet. Suppl., Abstract S22B-05.

CASTRO, R.R., MUCCIARELLI, M., PACOR, F., and PETRUNGARO, C. (1997), *S-wave site-response estimates using horizontal-to-vertical spectral ratios*, Bull. Seismol. Soc. Am. *87*(1), 256–260, 1997.

CHIN, B. and AKI, K. (1991), *Simultaneous study of the source, path, and site effects on strong ground motion during the 1989 Loma Prieta earthquake: A preliminary result on pervasive nonlinear site effects*, Bull. Seismol. Soc. Am. *81*, 1859–1884.

COCHRAN, E.S., VIDALE, J.E., and LI, Y.-G. (2003), *Near-fault anisotropy following the Hector Mine earthquake*, J. Geophys. Res. *108*(B9), 2436, doi:10.1029/2002JB002352.

CORMIER, V.F. and SPUDICH, P. (1984), *Amplification of ground motion and waveform complexities in fault zones: Examples from the San Andreas and the Calaveras faults*, Geophys. J. R. Astr. Soc. *79*, 135–152.

CRAMPIN, S. and GAO, Y. (2005), *Comment on "Systematic Analysis of Shear-Wave Splitting in the Aftershock Zone of the 1999 Chi-Chi, Taiwan, Earthquake: Shallow Crustal Anisotropy and Lack of Precursory Changes" by LIU, Y. Teng, T.-L., BEN-ZION, Y.*, Bull. Seismol. Soc. Am. *95*, 354–360.

CRAMPIN, S., BOOTH, D.C., EVANS, R., PEACOCK, S., and FLETCHER, J.B. (1990), *Change in shear-wave splitting at Anza near the time of the North Palm Springs earthquake*, J. Geophys. Res. *95*, 11197–11212.

CRAMPIN, S., BOOTH, D.C., EVANS, R., PEACOCK, S., and FLETCHER, J.B. (1991), *Comment on "Quantitative measurements of shear-wave polarizations at the Anza seismic network, Southern California: Implications for shear-wave splitting and earthquake prediction" by ASTER, R.C., Shearer, P.M., and Berger, J.*, J. Geophys. Res. *96*, 6403–6414.

DAS, S. and SCHOLZ, C.H. (1981), *Theory of time-dependent rupture in the earth*, J. Geophys. Res. *86*, 6039–6051.

DIETERICH, J.H. (1978), *Time-dependent friction and the mechanics of stick-slip*, Pure Appl. Geophys. *116*, 790–806.

DIETERICH, J.H. (1994), *A constitutive law for rate of earthquake production and its application to earthquake clustering*, J. Geophys. Res. *99*, 2601–2618.

DIETERICH, J.H. and KILGORE, B.D. (1996), *Imaging surface contacts; power law contact distributions and contact stresses in quarts, calcite, glass, and acrylic plastic*, Tectonophysics *256*, 219–239.

FIELD, E.H., JOHNSON, P.A., BERESNEV, I.A., and ZENG, Y., (1997), *Nonlinear ground-motion amplification by sediments during the 1994 Northridge earthquake*, Nature *390*, 599–602.

FOHRMANN, M., JAHNKE, G., IGEL, H., and BEN-ZION, Y. (2004), *Guided waves from sources out side faults: An indication of shallow trapping structure?*, Pure Appl. Geophys. *161*, 2125–2137.

GRET, A., SNIEDER, R., ASTER, R.C., and Kyle, P.R. (2005), *Monitoring rapid temporal change in a volcano with coda wave interferometry*, Geophys. Res. Lett. *32*, L06304, doi:10.1029/2004GL021143.

GOLDSTEIN, P., DODGE, D., FIRPO, M., and MINNER, L., *SAC2000: Signal processing and analysis tools for seismologists and engineers*. In *The IASPEI International Handbook of Earthquake and Engineering Seismology, Part B* (eds. Lee, W.H.K., KANAMORI, H., Jennings, P.C., and KISSLINGER C.) (Academic Press, London 2003), Chapter 85.5.

GOT, J. L., and COUTANT, O. (1997), *Anisotropic scattering inferred from travel-time delay analysis in Kilauea volcano, Hawaii, earthquake coda waves*, J. Geophys. Res. *102*, 8397–8410.

GUPTA, I.N. (1973), *Premonitory variations in S-wave velocity anisotropy before earthquakes in Nevada*, Science *182*, 1129–1132.

HAMIEL, Y., LIU, Y., LYAKHOVSKY, V., BEN-ZION, Y., and LOCKNER, D. (2004), *A Visco-elastic damage model with applications to stable and unstable fracturing*, Geophys. J. Int. *159*, 1155–1165, doi: 10.1111/j.1365-246X.2004.02452.x.

HARTLEB, R.D., DOLAN, J.F., AKYÜZ, H.S., DAWSON, T.E., TUCKER, A.Z., YERLI, B., ROCKWELL, T.K., TORAMAN, E., ÇAKIR, Z., DIKBAS, A., and ALTUNEL, E. (2002), *Surface rupture and slip distribution along the Karadere segment of the 17 August 1999 İzmit and the western section of the 12 November 1999 Düzce, Turkey, earthquakes*, Bull. Seismol. Soc. Am. *92*(1), 67–78.

HELLWEG, M., SPUDICH, P., FLETCHER, J. and BAKER, L.M. (1995), *Stability of coda Q in the region of Parkfield, California: The view from the USGS Parkfield dense seismograph array*, J. Geophys. Res. *100*, 2089–2102.

IGARASHI, T., MATSUZAWA, T. and HASEGAWA, A. (2003), *Repeating earthquakes and interplate aseismic slip in the northeastern Japan subduction zone*. J. Geophys. Res. *108*(B5), 2249, doi:10.1029/2002JB001920.

IKUTA, R. and YAMAOKA, K. (2004), *Temporal variation in the shear-wave anisotropy detected using the Accurately Controlled Routinely Operated Signal System (ACROSS)*, J. Geophys. Res. *109*, B09305, doi:10.1029/2003JB002901.

JAEGER, J.C. and COOK, N.G.W., *Fundamentals of Rock Mechanics* (Chapman and Hall, New York 1976).

JIN, A. and AKI, K. (1986), *Temporal change in coda Q before the Tangshan earthquake of 1976 and the Haicheng earthquake of 1975*, J. Geophys. Res. *91*, 665–673.

JOHNSON, P. and SUTIN, A. (2005), *Slow dynamics and anomalous nonlinear fast dynamics in diverse solids*, J. Acoust. Soc. Am. *117*, 124–130.

KANAMORI, H. and ANDERSON, D.L. (1975), *Theoretical basis of some empirical relations in seismology*, Bull. Seismol. Soc. Am. *65*, 1073–1095.

KANAMORI, H. and FUIS, G. (1976), *Variation of P-wave velocity before and after the Galway Lake earthquake (M_L = 5.2) and the Goat Mountain earthquakes (M_L = 4.7, 4.7), 1975, in the Mojave desert, California*, Bull. Seismol. Soc. Am. *66*, 2027–2037.

KASAHARA, K., *Earthquake Mechanics* (Cambridge University Press, New York 1981).

KLEIN, F.W. (1978), *Hypocenter location program HYPOINVERSE*, USGS, Open File Report, 78–694.

KISSLINGER, C. (1996), *Aftershocks and fault-zone properties*, Adv. Geophys. *38*, 1–36.

LEARY, P.C., CRAMPIN, S., and MCEVILLY, T.V. (1990), *Seismic fracture anisotropy in the Earth's crust: An overview*, J. Geophys. Res. *95*(7), 11105–11114.

LEWIS, M.A, PENG, Z., BEN-ZION, Y., and VERNON, F.L. (2005), *Shallow seismic trapping structure in the San Jacinto fault zone near Anza, California*, Geophys. J. Int. *162*(3), 867–881, doi: 10.1111/j.1365-246X.2005.02684.

LIU, Y., TENG, T.-L., and BEN-ZION, Y. (2004), *Systematic analysis of shear-wave splitting in the aftershock zone of the 1999 Chi-Chi earthquake: Shallow crustal anisotropy and lack of precursory variations*, Bull. Seismol. Soc. Am. *94*, 2330–2347.

LIU, Y., BEN-ZION, Y., and TENG T.-L. (2005), *Reply to Comment by Crampin and Gao on "Systematic Analysis of Shear-Wave Splitting in the Aftershock Zone of the Chi-Chi, Taiwan, Earthquake: Shallow Crustal Anisotropy and Lack of Precursory Changes," by LIU, Y. Teng, T.-L., and BEN-ZION, Y.*, Bull. Seismol. Soc. Am. *95*, 361–366.

LOCKNER, D. A., BYERLEE, J.D., KUKSENKO, V., PONOMAREV, A., and SIDORIN, A. (1992), *Observations of quasi-static fault growth from acoustic emissions*. In *Fault Mechanics and Transport Properties of Rocks,* International Geophysics Series (eds. Evans, B., and Wong, T.-f.) (Academic Press, San Diego, 1992) 51, 3–31.

LYAKHOVSKY, V., BEN-ZION, Y., and AGNON, A. (1997), *Distributed damage, faulting and friction*, J. Geophys. Res. *102*, 27635–27649.

LYAKHOVSKY, V., BEN-ZION Y., and Agnon, A. (2005), *A visco-elastic damage rheology and rate- and state-dependent friction*, Geophys. J. Int. *161*, 179–190, doi: 10.1111/j.1365-246X.2005.02583.x.

MARONE, C. (1998), *Laboratory-derived frictional laws and their application to seismic faulting*, Annu. Rev. Earth Planet. Sci. *26*, 643–696.

MATCHAM, I., SAVAGE, M.K., and GLEDHILL, K.R. (2000), *Distribution of seismic anisotropy in the subduction zone beneath the Wellington region, New Zealand*, Geophys. J. Int. *140*, 1–10.

MATSUMOTO, S., OBARA, K., YOSHIMOTO, T., SAITO, A., ITO, A., and HASEGAWA, A. (2001), *Temporal change in P-wave scatterer distribution associated with the M6.1 earthquake near Iwate volcano, northeastern* Japan, Geophys. J. Int. *145*, 48–58.

MCGUIRE, J. and BEN-ZION, Y. (2005), *High-resolution imaging of the Bear Valley section of the San Andreas Fault at seismogenic depths with fault-zone head waves and relocated seismicity*, Geophys. J. Int. *163*, 152–164, doi: 10.1111/j.1365-246X.2005.02703.x.

MOGI, K. (1962), *Study of the elastic shocks caused by the fracture of heterogeneous materials and its relation to earthquake phenomena*, Bull. Earthquake Res. Inst. Tokyo Univ. *40*, 125–173.

MCEVILLY, T.V. and JOHNSON, L.R. (1974), *Stability of P and S velocities from central California quarry blasts*, Bull. Seismol. Soc. Am. *64*, 343–353.

NADEAU, R.M., ANTOLIK, M., JOHNSON, P.A., FOXALL, W., and MCEVILLY, T.V. (1994), *Seismological studies at Parkfield III: Microearthquake clusters in the study of fault-zone dynamics*, Bull. Seismol. Soc. Am. *84*, 247–263.

NIU, F., SILVER, P.G., NADEAU, R.M., and MCEVILLY, T.V. (2003), *Stress-induced migration of seismic scatterers associated with the 1993 Parkfield aseismic transient event*, Nature *426*, 544–548.

NUTTLI, O. (1961), *The effect of earth's surface on the S-wave particle motio*n, Bull. Seismol. Soc. Am. *51*, 237–246.

OMORI, F. (1895), *On the aftershocks of earthquakes*, J. Coll. Sci. Imp. Univ. Tokyo. *7*, 111–200.

O'CONNELL, D.R.H. (1999), *Replication of apparent nonlinear seismic response with linear wave propagation models*, Science *283*, 2045–2050.

PAVLENKO, O.V. and IRIKURA, K. (2002), *Changes in shear moduli of liquefied and nonliquefied soils during the 1995 Kobe earthquake and its aftershocks at three vertical-array sites*, Bull. Seismol. Soc. Am. *92*, 1952–1969.

PAVLENKO, O.V. and IRIKURA, K. (2003), *Estimation of nonlinear time-dependent soil behavior in strong ground notion based on vertical array data*, Pure Appl. Geophys. *160*, 2365–2379.

PENG, Z., BEN-ZION, Y., MICHAEL, A.J., and ZHU, L. (2003), *Quantitative analysis of fault zone waves in the rupture zone of the Landers, 1992, California earthquake: Evidence for a shallow trapping structure*, Geophys. J. Int. *155*, 1021–1041.

PENG, Z. and BEN-ZION, Y. (2004), *Systematic analysis of crustal anisotropy along the Karadere-Düzce branch of the north Anatolian fault*, Geophys. J. Int. *159*, 253–274, doi: 10.1111/j.1365-246X.2004.02379.x.

PENG, Z. and BEN-ZION, Y. (2005), *Spatio-temporal variations of crustal anisotropy from similar events in aftershocks of the 1999 M7.4 İzmit and M7.1 Düzce, Turkey, earthquake sequences*, Geophys. J. Int. *160*(3), 1027–1043, doi: 10.1111/j.1365-246X.2005.02569.x.

PENG, Z., VIDALE, J.E., MARONE, C., and RUBIN, A. (2005), *Systemic variations in recurrence interval and moment of repeating aftershocks*, Geophys. Res. Lett. *32*(15), L15301, doi: 10.1029/2005GL022626.

PENG, Z. and VIDALE, J.E. (2004), *Early aftershock decay rates of the M6 Parkfield earthquake*, EOS Trans. AGU, *85*(47), Fall Meet. Suppl., Abstract S51C-0170X.

POUPINET, G., ELLSWORTH, W.L., and FRECHET, J. (1984), *Monitoring velocity variations in the crust using earthquake doublets: An application to the Calaveras Fault, California*, J. Geophys. Res. *89*, 5719–5731.

ROVELLI, A., CASERTA, A., MARRA, F., and RUGGIERO, V. (2002), *Can seismic waves be trapped inside an inactive fault zone? The case study of Nocera Umbra, Central Italy*, Bull. Seismol. Soc. Am. *92*, 2217–2232.

ROUMELIOTI, Z. and BERESNEV, I.A. (2003), *Stochastic finite-fault modeling of ground motions from the 1999 Chi-chi, Taiwan, earthquake: Application to rock and soil sites with implications for nonlinear site response*, Bull. Seismol. Soc. Am. *93*, 1691–1702.

REILINGER, R.E., MCCLUSKY, S.C., ORAL, M.B., KING, R.W., TOKSOZ, M.N., BARKA, A.A., KINIK, I., LENK, O., and SANLI, I. (1997), *Global Positioning System measurements of the present day crustal movements in the Arabia-Africa-Eurasia plate collision zone*, J. Geophys. Res. *102*, 9983–9999.

RUBIN, A.M. (2002), *Using repeating earthquakes to correct high-precision earthquake catalogs for time-dependent station delays*, Bull. Seismol. Soc. Am. *92*, 1647–1659.

RUBINSTEIN, J.L. and BEROZA, G.C. (2004a), *Evidence for widespread nonlinear strong ground motion in the M_w6.9 Loma Prieta earthquake*, Bull. Seismol. Soc. Am. *94*(5), 1595–1608.

RUBINSTEIN, J.L. and BEROZA, G.C. (2004b), *Nonlinear strong ground motion in the Ml5.4 Chittenden earthquake: Evidence that pre-existing damage increases susceptibility to further damage*, Geophys. Res. Lett. *31*, L23614, doi: 10.1029/2004GL021357.

RUBINSTEIN, J.L. and BEROZA, G.C. (2005). *Depth constraints on nonlinear strong ground motion*, Geophys. Res. Lett. *32*, L14313, doi:10.1029/2005GL023189.

RYALL, A. and SAVAGE, W. (1974), *S wave splitting: Key to earthquake prediction?* Bull. Seismol. Soc. Am. *64*, 1943–1951.

SAVAGE, M.K. (1999), *Seismic anisotropy and mantle deformation: What have we learned from shear-wave splitting*, Rev. Geophys. *37*, 65–106.

SCHAFF, D.P., BEROZA, G.C., and SHAW, B.E. (1998), *Postseismic response of repeating aftershocks*, Geophys. Res. Lett. *25*(24), 4549–4552.

SCHAFF, D.P., BOKELMANN, G.H.R., BEROZA, G.C., WALDHAUSER, F., and ELLSWORTH, W.L. (2002), *High-resolution image of Calaveras fault seismicity*, J. Geophys. Res. *107*(B9), 2186, doi:10.1029/2001JB000633.

SCHAFF, D. P., BOKELMANN, G.H.R., ELLSWORTH, W.L., ZANZERKIA, E., WALDHAUSER, F., and BEROZA, G.C. (2004), *Optimizing correlation techniques for improved earthquake location*, Bull. Seismol. Soc. Am. *94*, 705–721.

SCHAFF, D.P. and BEROZA, G.C. (2004), Coseismic and postseismic velocity changes measured by repeating earthquakes, J. Geophys. Res. *109*, B10302, doi:10.1029/2004JB003011.

SCHOLZ, C.H. (1968), *Microfracturing and the inelastic deformation of rock in compression*, J. Geophys. Res. *73*, 1117–1432.

SEEBER, L., ARMBRUSTER, J.G., OZER, N., AKTAR, M., BARIS, S., OKAYA, D., BEN-ZION, Y., and FIELD, E., *The 1999 earthquake sequence along the North Anatolia transform at the juncture between the two main ruptures.* In *The 1999 İzmit and Düzce Earthquakes: Preliminary Results* (eds. Barka *et al.*) (Istanbul Technical University, Turkey 2000) pp. 209–223.

SILVER, P.G. (1996), *Seismic anisotropy beneath the continents: probing the depths of geology*, Annu. Rev. Earth Planet. Sci. *24*, 385–432.

SNIEDER, R., (2006), *The Theory of Coda Wave Interferometry*, this volume.

SNIEDER, R. and VRIJLANDT, M. (2005), *Constraining the source separation with coda wave interferometry: Theory and application to earthquake doublets in the Hayward fault, California*, J. Geophys. Res. *110*, B04301, doi:10.1029/2004JB003317.

SNIEDER, R., GRET, A., DOUMA, H., and SCALES, J. (2002), *Coda wave interferometry for estimating nonlinear behavior in seismic velocity*, Science *295*, 2253–2255.

SPUDICH, P. and OLSEN, K.B. (2001), *Fault zone amplified waves as a possible seismic hazard along the Calaveras fault in central California*, Geophys. Res. Lett. *28*, 2533–2536.

TEN CATE, J.A. and SHANKLAND, T. (1996), *Slow dynamics in the nonlinear elastic response of Berea sandstone*, Geophys. Res. Lett. *23*, 3019–3022.

TEN CATE, J.A., SMITH, E., and GUYER, R.A. (2000), *Universal slow dynamics in granular solids*, Phys. Rev. Lett. *85*, 1020–1023.

UTKUCU, M., NALBANT, S.S., MCCLOSKEY, J., STEACY, S., and ALPTEKIN, O. (2003), *Slip distribution and stress changes associated with the 1999 November 12, Düzce (Turkey) earthquake (M_w = 7.1)*, Geophys. J. Int. *153*, 229–241.

VIDALE, J.E. and LI, Y.-G. (2003), *Damage to the shallow Landers fault from the nearby Hector Mine earthquake*, Nature *421*, 524–526.

WALDHAUSER, F. and ELLSWORTH W.L. (2000), *A double-difference earthquake location algorithm: Method and application to the northern Hayward fault, California*, Bull. Seismol. Soc. Am. *90*, 1353–1368.

WALDHAUSER, F. and ELLSWORTH, W.L. (2002), *Fault structure and mechanics of the Hayward fault, California, from double-difference earthquake locations*, J. Geophys. Res. *107*(B3), 2054, doi:10.1029/2000JB000084.

WALDHAUSER, F., ELLSWORTH, W.L., SCHAFF, D.P., and COLE, A. (2004), *Streaks, multiplets, and holes: High-resolution spatio-temporal behavior of Parkfield seismicity*, Geophys. Res. Lett. *31*, L18608, doi:10.1029/2004GL020649.

WESSEL, P. and SMITH, W.H.F. (1998), *New, improved version of the Generic Mapping Tools released*, EOS Trans. Amer. Geophys. Union *79*, 579.

WENNERBERG, L. (1996), *Comment on "Simultaneous study on the source, path, and site effects on strong ground motion during the 1989 Loma Prieta earthquake: A preliminary result on pervasive nonlinear site effects" by Chin, B.-H., and Aki, K.*, Bull. Seismol. Soc. Am. *86*, 259–267.

WHITCOMB, J.H., GARMANY, J.E. and ANDERSON, D.L. (1973), *Earthquake prediction: Variation of seismic velocities before the San Francisco earthquake*, Science *180*, 632–635.

YAMAWAKI, T., NISHIMURA, T., and HAMAGUCHI, H. (2004), *Temporal change of seismic structure around Iwate volcano inferred from waveform correlation analysis of similar earthquakes*, Geophys. Res. Lett. *31*, L24616, doi:10.1029/2004GL021103.

ZHU, X. (2003), *Management of large earthquake data using the antelope relational database and seismicity analysis of the 1999 Turkey earthquake sequences*, M.S. Thesis, 96 pp., University of Southern California, Los Angeles, California.

ZÖLLER, G., Hainzl, S., HOLSCHNEIDER, M., and BEN-ZION, Y. (2005), *Aftershocks resulting from creeping sections in a heterogeneous fault*, Geophys. Res. Lett. *32*, L03308, doi:10.1029/2004GL021871.

(Received April 5, 2005, accepted September 9, 2005)